TAMPERE UNIVERSITY OF TECHNOLOGY

TOMI PRIHTI

WEAR BEHAVIOUR OF DUCTILE IRONS IN CONTINUOUS SLIDING MOTION

Master of Science Thesis

Examiner: Professor Tuomo Tiainen
Examiner and topic approved in the Faculty of Automation, Mechanical and Materials Engineering meeting on 6. April 2011

ABSTRACT

TAMPERE UNIVERSITY OF TECHNOLOGY
Master's Degree Programme in Materials Science
PRIHTI, TOMI: Wear behaviour of ductile irons in continuous sliding motion
Master of Science Thesis, 58 pages, 7 Appendix pages
May 2011
Major: Metal Materials
Examiner: Professor Tuomo Tiainen
Keywords: ductile cast iron, sliding wear, pin-on-disk machine

This Master of Science thesis is carried out for Componenta Ltd. Componenta is one of the largest cast component suppliers in Europe. The thesis is also part of the DEMAPP research program launched by FIMECC Ltd. DEMAPP program develops novel breakthrough materials with improved performance for applications in demanding operational and service environments.

Ductile irons are considered to be ideal materials for a wide range of wear applications, especially frictional wear under both dry and lubricated conditions. However, the discussion of wear resistance of ductile irons is mostly limited to general level due to the large variety of test methods, with each test concentrating to a specific set of conditions. The aim of this Master of Science thesis is to study the wear of different ductile iron grades in continuous sliding motion against steel. The main goal is to get comparable information on wear resistance and wear behaviour of selected ductile irons under specific conditions.

The theoretical part is discussing the properties of the studied materials and wear phenomena. The general wear mechanisms and variables influencing wear are presented along with the existing knowledge on the wear of ductile irons on the basis of literature review.

The experimental work consists of sample preparation and sample holder design, preliminary and actual wear tests and of the analysis of worn samples. The wear tests are run in VTT Otaniemi with a pin-on-disc tribotester using special sample geometry. The studied ductile irons are used as disc material and steel wire as pin material. The total number of 10 different EN-standard ductile iron grades are used in the wear tests, including austempered and solution strengthened grades. The tests are carried out under dry and lubricated conditions using constant test parameters.

According to the wear test results, austempered grades seem to wear much slower than the others. In fact, the wear rate was found to be negative, indicating that there is more material transferred into the surface of ADI discs than has been worn off. This is understandable, as the pin wear was increased along with the hardness of the disc. The novel high silicon ductile iron grades also showed promising wear results both under dry and lubricated sliding conditions. There was also an intention to study the actual wear mechanisms with SEM, but due to a lack of time this will be carried out as an additional study.

TIIVISTELMÄ

TAMPEREEN TEKNILLINEN YLIOPISTO
Materiaalitekniikan koulutusohjelma
PRIHTI, TOMI: Pallografiittivalurautojen kulumiskäyttäytyminen jatkuvassa liukuvassa liikkeessä
Diplomityö, 58 sivua, 7 liitesivua
Toukokuu 2011
Pääaine: Metallimateriaalit
Tarkastaja: professori Tuomo Tiainen
Avainsanat: Pallografiittivalurauta, liukuva kuluminen, tappikulutustesti

Tämä diplomityö on tehty Componenta Oyj:n toimeksiannosta. Componenta on Euroopan suurimpia valukomponenttien tuottajia. Diplomityö on myös osa FIMECC Oy:n hallinnoimaa DEMAPP -hanketta. Hankkeen tavoitteena on kehittää uusia kilpailukykyisiä materiaaleja vaativiin käyttöolosuhteisiin.

Pallografiittivalurautoja pidetään ihanteellisina materiaaleina moneen eri kulumistilanteeseen, erityisesti hankaavaan kulumiseen sekä voitelemattomana että voideltuna. Pohdinta pallografiittivalurautojen kulumiskestävyydestä jää kuitenkin usein yleiselle tasolle: testimenetelmiä ja –olosuhteita on hyvin monenlaisia. Diplomityön tavoitteena on tutkia eri pallografiittivalurautalaatujen kulumista jatkuvassa liukuvassa liikkeessä terästä vasten puristettuna. Tärkeimpänä tavoitteena on saada vertailukelpoista tietoa tutkittavien valurautojen kulumiskestävyydestä ja –käyttäytymisestä työssä tutkituissa olosuhteissa.

Työn teoriaosuus käsittelee tutkittavien materiaalien ominaisuuksia ja kulumisilmiöitä. Keskeiset kulumismekanismit ja kulumiseen vaikuttavat tekijät esitellään yhdessä jo olemassa olevien tutkimustulosten kanssa.

Työn kokeellinen osuus koostuu näytteiden valmistuksesta, näytteenpitimien suunnittelusta ja rakentamisesta, kulutuskokeista esikokeineen sekä kuluneiden näytteiden analysoinnista. Kulutuskokeet suoritettiin tappikulutuskoneella VTT:n tribologian laboratoriossa Otaniemessä. Kokeissa käytettiin tavanomaisesta poikkeavaa näytegeometriaa, koska tappina toimi taivutettu teräslanka. Tutkittavat pallografiittivaluraudat puolestaan toimivat kiekkomateriaalina. Kaikkiaan kokeissa testattiin kymmenen eri EN-standardin mukaista valurautalajia, mukaan lukien austemperoidut ja liuoslujitetut lajit. Kulutuskokeet suoritettiin vakioparametrein sekä kuivana että voideltuna.

Kulutuskokeiden perusteella austemperoidut lajit kuluvat tutkitussa koetilanteessa vähemmän kuin muut rautalajit. Itse asiassa kuluminen ADI-lajeilla oli negatiivista, mikä viittaa siihen, että enemmän vastinparin materiaalia on tarttunut kiekon pintaan kuin kulunut pois. Tämä on ymmärrettävää, sillä tapin kuluminen näytti lisääntyvän samalla kun kiekon kovuus kasvoi. Myös uusi liuoslujitettu pallografiittivalurauta antoi lupaavia tuloksia sekä voidelluissa että voitelemattomissa olosuhteissa. Tarkoituksena oli myös tutkia vaikuttavia kulumismekanismeja SEM-mikroskoopilla, mutta ajan puutteen vuoksi tämä tarkastelu tehdään diplomityön ulkopuolella.

PREFACE

This thesis work is carried out as a part of the Master's Degree Programme in Materials Science in Tampere University of Technology, Finland. I would like to thank all people who have supported me during my studies and especially with this thesis.

I want to thank my examiner professor Tuomo Tiainen for the guidance and the criticism concerning the thesis. I am also grateful to Componenta Oyj and my mentor Mikko Mykrä for all the help I have received and for the opportunity to work with this interesting subject.

I thank Peter Andersson of VTT for the support and expertise through the thesis and especially in the experimental part.

In addition, I would like to thank my family for ongoing support during my studies. Finally my special thanks go to my fiancée Annu for the priceless support she gave me during my studies.

Tampere Finland, April 19, 2011 Tomi Prihti

TABLE OF CONTENTS

TERMS AND DEFINITIONS

ADI	Austempered Ductile Iron. Steel-like properties produced by austempering.
BCC	Body centered cubic crystal
CAD	Computer aided design
CE	Carbon equivalent
COF	Coefficient of friction
DEMAPP	A program launched by FIMECC. The main research targets for the program are wear-related phenomena and material requirements for demanding operational environments.
FCC	Face centered cubic crystal
FIMECC	Finnish metals and engineering competence cluster. Works to boost strategic research on metals and engineering industries.
HCP	Hexagonal close packed crystal
HICON	High friction and low wear contacts. A subproject of DEMAPP.
Pin-On-Disc	A tribotester using two different specimens: a pin and a disc.
RPM	Revolutions per minute
SWR	Specific wear rate (typically quoted as mm^3 / Nm)
VTT	Technical Research Center of Finland

1 INTRODUCTION

Ductile irons have turned out to be excellent materials for a wide range of industrial applications, where good wear resistance is needed. Wear is a complex phenomenon and it is influenced by material, operational, geometric and environmental variables. The main goals of the thesis are to get comparable information on the wear and friction behaviour of different ductile iron grades and to use this information for finding new material alternatives for definite industrial applications. This thesis is concentrating on frictional sliding wear with and without lubrication. The experimental tests are carried out with a pin-on-disc tribotester. Due to the large number of studied materials, the variables in the wear tests are kept constant, except the sliding distance which is increased in lubricated tests.

The pin-on-disc tribotester is used to simulate continuous sliding wear between two different samples. In this work the ductile iron is used as a rotating disc and steel wire as a pin, which is in contact with the disc under a constant load. The pin geometry used in the wear tests differs from typical pin geometry since the steel wire is bent. During the test, the apparatus measures the frictional force of the contact and when the test is finished the wear rate of the samples can be evaluated from microscopic images and from the surface profile scanning results of the disc.

In the theoretical part the ductile iron family and wear phenomena are shortly introduced. Wear of ductile irons is discussed in the literature review at the end of the theoretical part. The experimental part explains the wear test procedures, sample preparation, test apparatus and sample measurements in detail. The results are presented and discussed in three categories; pin wear, disc wear and friction behaviour. The last section presents the conclusions of the thesis.

2 THEORETICAL BACKGROUND

2.1 Cast iron

Iron castings have been produced in various compositions for more than 2000 years. The iron foundry industry produces invisible yet vital products, because most iron castings are further processed, assembled and sold as components of other machinery, equipment and consumer items. Term "cast iron" does not refer to a single material, but to a family of materials where the major constituent is iron with important amounts of carbon and silicon. Cast irons are natural composite materials whose properties are determined by their microstructures. The continuous metal matrix and the chemical and morphological forms taken by carbon are the major microstructural constituents of cast irons. Carbon, silicon and phosphorus are graphitizers and their combined effect on graphite formation is defined by the so-called carbon equivalent (CE). The most common formula for carbon equivalent is presented in equation (1). Carbon equivalent value of 4.26 % corresponds to the eutectic composition [1].

$$CE = \%C + \frac{(\%Si + \%P)}{3} \qquad (1)$$

The usual composition of each cast iron type is given in Table 1 [2]. Cast irons with carbon content higher than the eutectic point are called hypereutectic and cast irons with lower carbon content are called hypoeutectic cast irons. Carbon and silicon largely determine the microstructure of cast products immediately after solidification. [1, 2, 3]

Table 1. *The compositional ranges and microstructures for different cast iron types [2].*

Type	C range (wt.%)	Si range (wt.%)	CE range	Usual composition	Eutectic product	Graphite shape	Common RT matrix microconstituents
Gray	2.5–4.0	1.0–3.0	2.8–5	Hypo	γ + graphite	Platelets	Ferrite, pearlite
Ductile	3.0–4.0	1.8–2.8	3.6–4.9	Hyper	γ + graphite	Spheres	Ferrite, pearlite, ausferrite
Malleable	2.0–2.6	1.1–1.6	2.4–3.2	Hypo	γ + carbide	"Popcorn"	Ferrite, pearlite
White	1.8–3.6	0.5–1.9	2–4.3	Hypo	γ + carbide		Ferrite, pearlite
Compacted	3.0–4.0	1.8–2.8	3.6–4.9	Eutectic	γ + graphite	Rods	Ferrite, pearlite

The presence of trace elements, addition of alloying elements, modification of solidification behaviour and heat treatment after solidification are used to modify the microstructure of cast iron to produce the desired mechanical properties in the following common types of cast iron: gray iron, ductile iron, white iron, malleable iron and compacted iron [3]. The experimental part of this thesis is dealing with ductile iron and its

two modifications, austempered ductile iron and solution strengthened ductile iron. These cast iron types are presented in more detail in the following chapters.

2.2 Ductile iron

2.2.1 History

The eternal dream of foundrymen became true in 1948 when H. Morrogh of the British Cast Iron Research Association announced that by adding a small amount of cerium to hypereutectic grey cast iron, a casting containing spherical graphite particles can be achieved [4]. Within the same year, the International Nickel Company (INCO) revealed that by using magnesium as a spheroidizer, a cast iron with similar structure could be obtained. INCO received a patent for ductile iron in year 1949 [3]. This was the beginning of the triumph of ductile iron.

2.2.2 Microstructure

Ductile iron, also known as spheroidal iron or nodular iron, is made by treating the liquid cast iron with suitable composition with magnesium before casting. This promotes the graphite to precipitate in the form of discrete nodules instead of interconnected flakes. The mechanism of solidification is entirely different from that of grey cast irons. This is resulting in a wide range of grades with tensile properties that are substantially higher than the grey cast iron can achieve. This difference in properties results from the differences in graphite morphology. Unlike graphite flakes, the graphite spheroids do not act as stress concentrators because they approach the optimum in terms of surface area to volume ratio. The matrix structure in ductile iron can be varied ranging from fully ferritic to fully pearlitic by the controlled selection of raw materials, alloying and heat treatment. The matrix dictates the tensile properties of ductile irons. [3, 5]

The Spheroidity, also known as the nodularity of graphite particles is defined as the percentage of graphite particles which are spheroidal or nodular in shape (form VI and V of EN ISO 945-1). EN ISO 945-1 [6] designates six forms of graphite defined as forms I to VI. The determination of the spheroidal form and its percentage are carried out by comparing a microscopic image of the studied material to reference pictures. The computer aided image analysis can be applied as well. A common requirement is the level of nodularity of 90 %; this generally ensures that the minimum tensile properties required in standards are reached, as long as the matrix of the chosen grade is adjusted accordingly. However, the mechanical properties may not be seriously affected until a significant deterioration in graphite form occurs. The nodule count also has an influence on the mechanical properties of ductile iron. Generally, high nodule count indicates good metallurgical quality, with each section size having an optimum range of nodule count. [3, 5, 7]

The mechanical properties of ductile iron are determined primarily by the matrix constituents and their hardness if the nodularity and nodule count are appropriate and

the porosity and carbide content are low. The matrix consists of ferrite and/or pearlite in the common grades of ductile iron. Ferrite is the purest iron phase in ductile iron. It has low strength and hardness, but high ductility and toughness. It is also easy to machine. Pearlite is a mixture of lamellar cementite in a ferritic matrix. Pearlite provides a combination of higher strength and hardness with lower ductility when compared to ferrite. The mechanical properties are determined by the ratio of ferrite to pearlite in the matrix. This ratio can be controlled in the as-cast condition by controlling the composition of the iron and also by adjusting the cooling rate of the casting. A fully ferritic casting can be obtained by heat treatment. The maximum pearlite content is achieved by normalizing heat treatment. Figure 1 [8] shows the typical microstructures of different types of ductile iron. All images in Figure 1 are etched with 4 % Nital in order to reveal the phase boundaries. [3, 8]

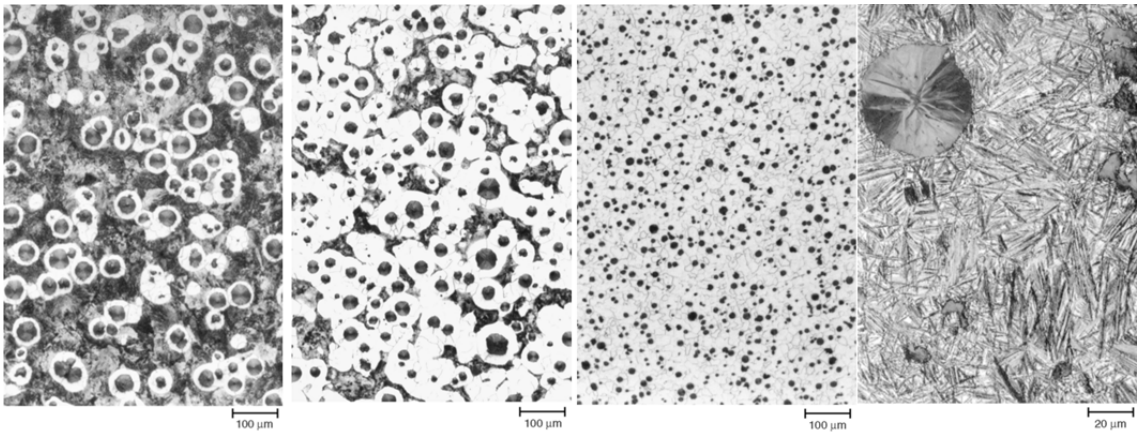

Figure 1. *Optical microscopy images of different ductile iron types from left to right; pearlite matrix with ferritic halos around the graphite nodules, ferritic/pearlitic matrix, ferritic matrix and ADI with acicular ferrite and austenite matrix. [8]*

The solidification process of ductile iron may be studied with the Fe-C phase diagram shown in Figure 2. [9] The dashed lines represent the existence limits of the stable phases and the solid lines indicate the metastable ones. The metastable diagram is more interesting from the cast iron point of view because normally the stable conditions take a long time to develop. As can be seen in Figure 2.2.1, pure iron melts at 1538° C and it can exist in three different crystal forms; α-iron called ferrite up to 912° C, γ-iron called austenite between 912° - 1394° C and δ-iron between 1394° - 1538° C. Ferrite has BCC crystal structure and it can dissolve only 0.02 % carbon in metastable system. Crystallographic structure of austenite is FCC and it can dissolve 2.08 % carbon. Cementite, Fe_3C, is a chemical compound of iron and carbon, iron carbide. Cementite is brittle and very hard and its crystallographic structure is quite complex. [1]

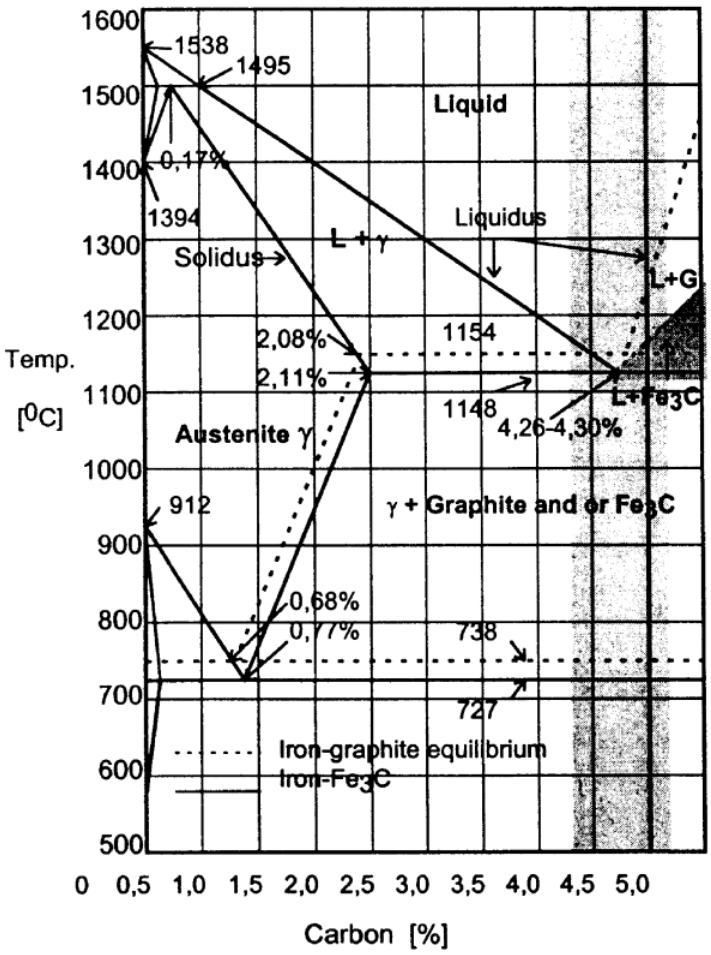

Figure 2. *The Fe-C binary phase diagram. [9]*

2.2.3 Chemical composition

Ductile iron is a ternary Fe-C-Si alloy. Standards ISO 1083 and EN 1563 do not specify requirements for metal composition; it is left to the discretion of the manufacturer. The selection of the composition depends on the section size of the casting and on the targeted mechanical properties. Although the nodule formation is mainly controlled by carbon and silicon contents, the purity level of the alloy and the addition of spheroidizing materials have a big influence on the formation of nodules. However, the carbon and silicon contents and cooling parameters control the amount of graphite embedded in the metallic phases. In principle, the property requirements of all the grades can be achieved using a fairly narrow range of carbon and silicon contents. In practice, most manufacturers operate close to the eutectic value. [5, 9]

The effects of graphitizing elements are various. Silicon decreases carbon solubility in austenite, increases the stable eutectic temperature, promotes the precipitation of graphite and increases the interval between the stable and metastable eutectic temperatures. Consequently it favors the graphite-austenite system. Silicon also increases the hardness, ultimate tensile strength and yield strength of the matrix but reduces its elongation and toughness, when existing in solid solution in ferrite. At room temperature the

solubility of silicon in ferrite can reach the value of 4 % [10]. Addition of silicon as an inoculant in the form of ferrosilicon (FeSi) has an increasing effect on the number of nucleation sites and on the nodule count. Consequently, it reduces the carbon diffusion path during the eutectoid transformation and increases the amount of ferrite in the structure. [9]

Sulfur has a major influence on the nucleation and growth of the graphite particles. Sulfur is a surface active element and can be absorbed by the graphite crystal. It favors the formation of flaky graphite particles instead of nodules. Ductile irons are sensitive for sulfur content: too high content may result in the formation of flake graphite while too low content may result in a smaller number of nodules. The recommended content of sulfur is between 0.010 and 0.015 weight percentage. [9]

Even though phosphorus promotes graphite formation, it is classified as a deleterious element in ductile iron. Phosphorus enhances the formation of pearlite and increases the hardness and tensile strength but reduces the elongation. The control of this element is crucial for achieving high mechanical properties, especially impact resistance. The phosphorus content of ductile irons is usually smaller than 0.04 %. [5, 9]

The carbon crystallization as graphite spheroids is the result of the action of definite elements. Magnesium, calcium, yttrium and rare earths provide the necessary conditions for the precipitation of the spheroidal graphite nodules. Their role is to neutralize the surface active elements i.e. sulfur and oxygen. The most common spheroidizing element is magnesium, because it is cheap and applicable for a wide range of CE values and casting sections. The main role of calcium is to reduce the volatility of the magnesium reaction and to improve the recovery of magnesium. [9]

2.2.4 Alloying elements

The structure and properties of ductile iron can be modified by alloying elements. The effects of major alloying elements are summarized in table 2. The required amount of pearlite can be obtained with alloying elements. The most common pearlite promoting elements are copper and tin. Tin is about 10 times more effective pearlite promoter than copper. Tin segregates to the surface of the graphite nodules and acts as a barrier to the transfer of carbon atoms to the graphite particles. Copper is normally used, however, because it increases the tensile strength and maintains a higher ductility than tin. Excessive addition of pearlite promoting elements leads to increased embrittlement. [5, 9]

Table 2. *The effects of alloying elements on ductile iron. [9]*

	Max. recommended ranges	Effects on stable and metastable eutectic T	Effects on eutectoid T	Effect on matrix structure	Effect on hardenability	Effect on graphite structure	Segregation direction
Cu	from 0.03% in ferritic to 1% in pearlitic	Increases the difference between stable and metastable eutectic temperatures	Reduces eutectoid temperature (austenite stabilizer)	Promotes pearlite by retarding C diffusion. Stabilizes pearlite	Raises hardenability but less effective than Mo	Promotes intercellular flake when in combination with Ti or Pb [23]	First liquid to freeze negatively segregating element
Ni	from 0.1% in ferritic to 0.25% in pearlitic	Increases the difference between stable and metastable eutectic temperatures	Reduces eutectoid temperature (austenite stabilizer)	Promotes pearlite weakly	Raises hardenability but less effective than Cu	Chunky graphite, reduces the tendency to chill	First liquid to freeze negatively segregating element
Mo	from 0.02% in ferritic to spec. in pearlitic	Lowers both eutectic temperatures	Increases eutectoid temperature (ferrite stabilizer)	Promotes pearlite in as-cast, less effective than Cu and Sn	Raises hardenability, the more effective element by delaying pearlite formation	Weak intercellular carbide former ** which are not broken down by heat treatment	Towards last liquid to freeze
Mn	from 0.15% in ferritic to 0.35%* in pearlitic	Lowers both eutectic temperatures	Reduces eutectoid temperature (austenite stabilizer)	Promotes pearlite, five times more effective than Ni	Raises hardenability, delays pearlite formation to lower T	Intercellular carbide network if segregation occurs in thick sections	Towards last liquid to freeze

2.2.5 Different grades of ductile iron

Ductile irons form a really versatile family of materials offering a wide range of properties obtained through microstructural control. Mechanical properties can be tailored for either high elongation or high strength or for a compromise between them. There are various standards for ductile irons. In this thesis the applied standards are limited to EN and ISO standards, because they are the most widely used and the test samples in the experimental part are cast according to these standards. The ductile irons used in the wear tests of this thesis are cast according to the EN 1563 European standard. Austempered grades follow the requirements of the EN 1564 standard and the solution strengthened ferritic ductile irons meet requirements of the preliminary standard prEN 1563, which includes the novel high silicon grades. Table 3 presents the standard ductile iron grades and their tensile properties. [3]

Table 3. *Mechanical properties of different ductile iron grades according to EN 1563. [11]*

Material designation		Tensile strength R_m N/mm^2	0,2 % proof stress $R_{p0,2}$ N/mm^2	Elongation A %
Symbol	Number	min.	min.	min.
EN-GJS-350-22-LT [1)]	EN-JS1015	350	220	22
EN-GJS-350-22-RT [2)]	EN-JS1014	350	220	22
EN-GJS-350-22	EN-JS1010	350	220	22
EN-GJS-400-18-LT [1)]	EN-JS1025	400	240	18
EN-GJS-400-18-RT [2)]	EN-JS1024	400	250	18
EN-GJS-400-18	EN-JS1020	400	250	18
EN-GJS-400-15	EN-JS1030	400	250	15
EN-GJS-450-10	EN-JS1040	450	310	10
EN-GJS-500-7	EN-JS1050	500	320	7
EN-GJS-600-3	EN-JS1060	600	370	3
EN-GJS-700-2	EN-JS1070	700	420	2
EN-GJS-800-2	EN-JS1080	800	480	2
EN-GJS-900-2	EN-JS1090	900	600	2

Ferritic ductile iron grades are ductile and impact resistant with tensile and yield strength values equivalent to those of low carbon steels. Ferritic ductile irons can be used in as-cast condition but they may be annealed to ensure maximal ductility and low temperature toughness. Ferritic-pearlitic ductile irons are normally cast without heat treatment. They are the most commonly used ductile iron grades having a matrix containing both ferrite and pearlite. Mechanical properties are intermediate between ferritic and pearlitic grades, combined with low production costs and good machinability. Pearlitic ductile irons have high strength, good wear resistance but moderate ductility and impact resistance. [3]

2.3 Austempered ductile iron

Austempered ductile iron, also known as ADI, is based on a Finnish invention. ADI was developed in the early 1970's at the Högfors foundry of Kymi-Kymmene Ltd. in Karkkila. In 1972 it was granted a patent in 13 countries as a special cast iron called Kymenite. Heat treatment is a crucial part of ADI production. Before heat treatment ADI is ductile iron with a combination of alloying elements which are used to achieve the desired hardenability in ADI. The particular microstructure of ADI offers a unique combination of tensile and fatigue strength values, ductility, toughness, wear resistance and machinability in conjunction with design flexibility and low cost. The mechanical properties of different ADI grades are presented in table 4. This table shows the minimum strength and ductility values that are required from each ADI grade in the European standard EN 1564. The standard does not define the chemical composition or heat treatment parameters, these are left to foundries to decide. Table 5 presents the hardness

ranges of different ADI grades in Brinell units. The range of hardness for each grade reflects the influence of wall thickness on the mechanical properties. [3, 12, 13]

Table 4. *Mechanical properties of different ADI grades according to the standard EN 1564. [13]*

Material designation		Tensile strength R_m N/mm^2	0,2 % proof stress $R_{p0,2}$ N/mm^2	Elongation A %
Symbol	Number	min.	min.	min.
EN-GJS-800-8	EN-JS1100	800	500	8
EN-GJS-1000-5	EN-JS1110	1000	700	5
EN-GJS-1200-2	EN-JS1120	1200	850	2
EN-GJS-1400-1	EN-JS1130	1400	1100	1

Table 5. *Hardness ranges of different ADI grades according to the standard EN 1564. [13]*

Material Designation		Brinell hardness range
Symbol	Number	HB
EN-GJS-800-8	EN-JS1100	260 to 320
EN-GJS-1000-5	EN-JS1110	300 to 360
EN-GJS-1200-2	EN-JS1120	340 to 440
EN-GJS-1400-1	EN-JS1130	380 to 480

The matrix structure in ADI is ausferritic which means that it is a combination of acicular ferrite and carbon stabilized austenite. The austenite in the ADI is stabilized by carbon during heat treatment and does not transform to brittle martensite even at sub-zero temperatures. Under high normal forces, thermodynamically stable austenite can undergo a strain-induced transformation which remarkably increases the wear resistance of ADI. The strain induced transformation generates a localized increase in volume and creates high compressive stresses which inhibit crack formation and growth and improve the fatigue properties of ADI. The increase in the wear resistance of ADI could be also due to work hardening of FCC austenite. [3]

The composition of ADI is little bit different from that of a conventional ductile iron. When considering the composition of both ADI and other ductile iron grades, the elements which adversely influence the quality of casting through the production of non-spheroidal graphite, or through the formation of carbides and inclusions or through the promotion of shrinkage, should be limited. The control of alloying elements influencing the hardenability of the iron along with the section size and the cooling rate of the austempering quench are also important to consider. Copper, nickel and molybdenum are the alloying elements used to increase the hardenability of ADI. Different combinations of these alloying elements are often used to achieve the desired hardenability, to avoid metallurgical problems or just for economic reasons. The hardenability of the matrix needs to be increased sufficiently to ensure that the formation of pearlite is avoided during the austempering process. [3]

ADI is produced by an isothermal heat treatment called austempering. Figure 3 presents typical austempering cycles for different grades of ADI. In the beginning the casting is heated to the austenization temperature in the range of 815 - 927° C. Then the casting is held for a sufficient time at this temperature to saturate the austenite with carbon. After that the casting is quenched to the austempering temperature in the range of 232 - 400° C. This needs to be done rapidly enough to avoid the formation of pearlite in the matrix. Austempering produces a matrix structure of ausferrite with about 2 % carbon content in the austenite. Finally the casting is cooled to the room temperature. A high temperature salt bath is a common way to accomplish the austempering. [3]

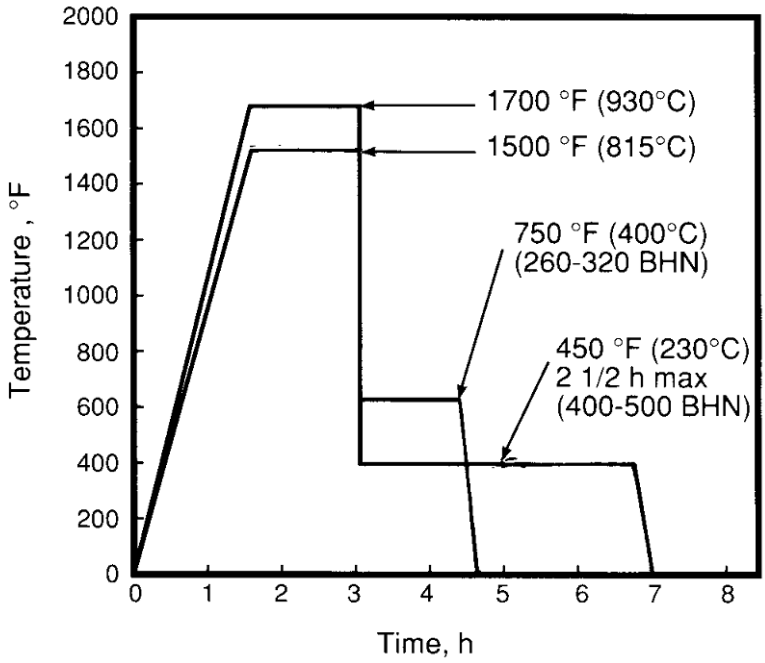

Figure 3. *Typical austempering parameters for different ADI grades. [3]*

2.4 Solution strengthened ductile iron

Solution strengthened ductile iron is a novel cast iron material included in the EN 1563 standard in year 2009. The standard is still in the preliminary stage and it is therefore called prEN 1563:2009. The solid solution strengthened ferritic grades present equivalent tensile strength values with higher proof strength and elongation values than those of the ferritic and pearlitic grades. The reduced hardness variation is one of the most significant properties of these solid solution strengthened grades. As a result, the machinability of castings is improved. The difference between the solution strengthened ductile iron and conventional ductile iron grades is in the silicon content, which is higher in the novel iron. Silicon content of GJS-500-14 is approximately 3.8 % and with GJS-600-10 it is 4.3 %. The matrix should be predominantly ferrite, with a maximum pearlite content of 5 %. The amount of free cementite should be limited to 1 %. Compacted graphite (form III) may be shown in heavy sections due to the increased silicon content. However, European standard accepts 20 % of form III graphite if the remainder

is mainly of form VI and V and the minimum tensile properties are fulfilled. Characteristic features of solution strengthened ferritic ductile iron grades are significantly higher proof strength and equal hardness values as compared to ferritic-pearlitic ductile irons, as shown in Figure 4. Table 6 presents the mechanical properties measured on test pieces machined from cast samples for the solution strengthened ferritic ductile iron according to prEN 1563: 2009. [7]

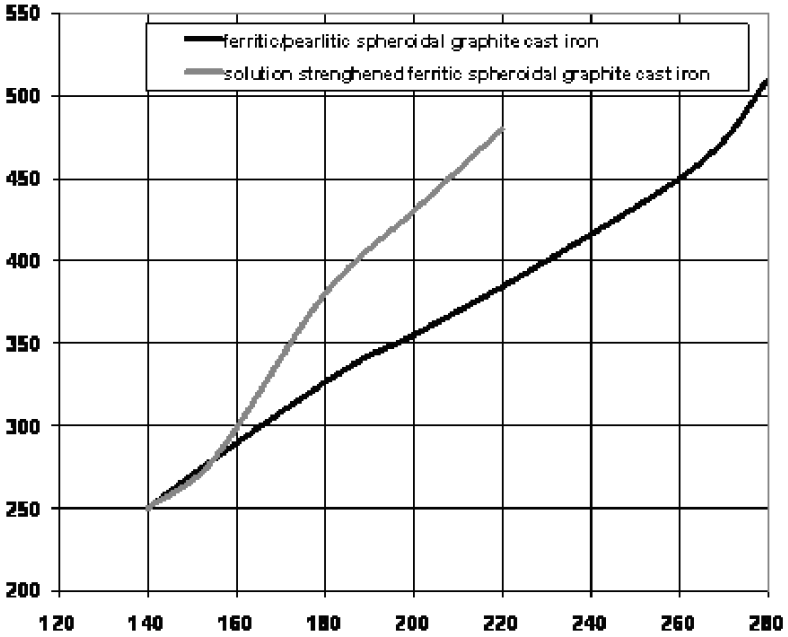

Figure 4. *Proof strength Rp0.2 values (N/mm2) of solution strengthened ferritic and ferritic/pearlitic ductile irons in function of Brinell hardness (HB). [7]*

Table 6. *The mechanical properties of solution strengthened ferritic ductile iron grades. [7]*

Material designation		Relevant wall thickness	0,2 % proof stress	Tensile strength	Elongation
		t	$R_{p0,2}$	R_m	A
		mm	MPa	MPa	%
Symbol	Number		min.	min.	min.
EN-GJS-450-18	5.3108	$t \leq 30$	350	450	18
		$30 \leq t \leq 60$	340	430	14
		$t > 60$	a	a	a
EN-GJS-500-14	5.3109	$t \leq 30$	400	500	14
		$30 \leq t \leq 60$	390	480	12
		$t > 60$	a	a	a
EN-GJS-600-10	5.3110	$t \leq 30$	450	600	10
		$30 \leq t \leq 60$	430	580	8
		$t > 60$	a	a	a

[a] To be agreed between the manufacturer and the purchaser.

2.5 Wear in sliding contacts

Wear means the damage on or the removal of material from the surface when solid parts are in sliding, rolling, or impact motion in relation to each other. Wear can affect either one or both of two solid surfaces. Wear damage precedes the actual loss of material, and it may also occur independently despite the fact that generally the definition of wear is based on the loss of material. Several parameters influence the wear and their simultaneous control is difficult. However, there is usually a leading mechanism that is mainly responsible for the wear. [14, 15]

Wear is not only a material property, it depends also on the operating system. Sometimes it is erroneously assumed that high-friction interfaces exhibit high wear rates. For instance, with solid lubricants there can be relatively low friction values combined with relatively high wear rate. Usually wear is an undesirable phenomenon in all applications but when controlled wear is required it can also be a good thing. For example in sliding bearings the run-in wear levels off the surface roughness and improves the operating conditions. [14]

The consequences of wear processes are usually described by wear rate. Wear rate is defined as the volume of material removed per sliding distance unit and normal force. This will be introduced in more detail in chapter 2.6.1. The reciprocal of wear rate is called wear resistance. It measures how well body resists the removal of material by wear processes. The used units depend on the type of wear and on the nature of the tribosystem. Also dimensionless forms of wear rate are used. Normally the wear rate is a complex function of time. It may start as low and later increase or vice versa as shown in Figure 5, where three hypothetical cases of worn volume as a function of sliding distance are presented. After a definite time, the wear rate remains constant for a period and it may change if the transition from one mechanism to another occurs during the wear test. The initial period is known as the run-in stage. During this period wear depends on the structure and properties of the initial material and its surface. Surface conditions such as surface finish have also an influence on wear. The surface roughness is modified to a steady-state condition by plastic deformation occurring during the transition run-in period. Initial conditions influence the duration of the transition period. Figure 6 shows the progress of wear loss depending on the predominant wear mechanism. A linear range in wear loss versus the operating time can be expected only during abrasive wear. The other three mechanisms may dominate in the sliding wear which usually produces the general three period wear pattern. [14, 15, 16]

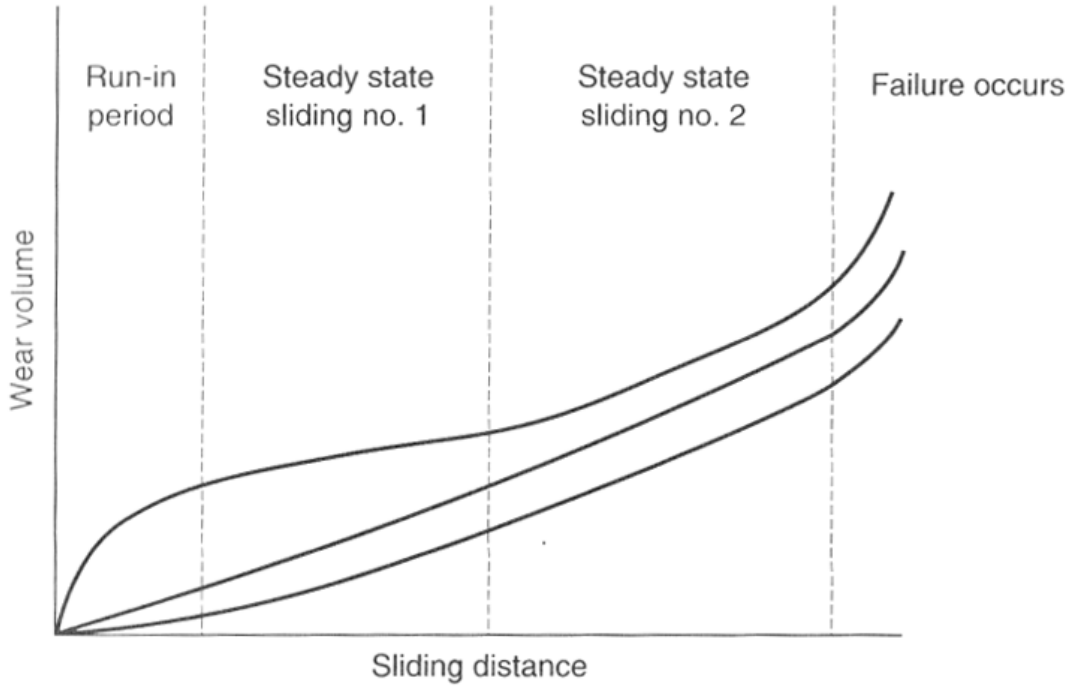

Figure 5. *Three hypothetical cases of wear loss as a function of sliding distance. [14]*

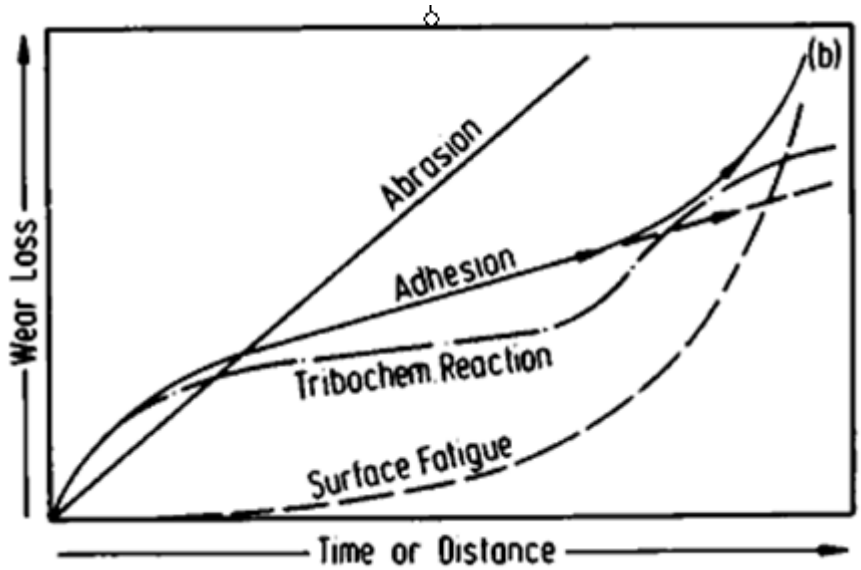

Figure 6. *The progress of wear loss as a function of operating time or sliding distance depending on the predominant wear mechanism. [16]*

There are several different classifications for wear mechanisms. Classification methods can be divided according to two basic viewpoints: the types of contact interactions between solid surfaces and the types of the relative motion of the contacting bodies. Wear according to the relative motion can be described as sliding wear, rolling wear, impact wear, fretting wear or slurry wear. These descriptions of wear do not represent the wear mechanisms in a scientific way; they are only based on the appearance of the contact type. From the contact interaction viewpoint the wear can be divided into

four fundamental modes: adhesive wear, abrasive wear, fatigue wear and corrosive wear. For example, the sliding wear may include all of these four wear modes. The four major wear mechanisms are explained in detail in chapter 2.6. [17, 18]

2.6 Wear mechanisms

2.6.1 Adhesive wear

Adhesive wear occurs when two nominally flat solid surfaces are in sliding contact, whether as lubricated or not. Adhesive wear is schematically shown in Figure 7. Adhesion occurs at the asperity contacts at the interface. These contacts are sheared by sliding which may result in the detachment of a wear particle from one of the surfaces and its attachment to the other surface. This type of wear occurs when there is enough adhesive bonding across the contact interface. When the adhesive bonding strength resists the relative sliding, large plastic deformation caused by dislocation glide is introduced in the contact region due to the compression and shearing. As a result, a crack is initiated and it propagates in the combined tensile and shearing fracture modes. A wear particle is formed when the crack reaches the contact interface. The transferred fragments may come off from the surface as the sliding continues and they can even be transferred back to the original surface. [14, 17]

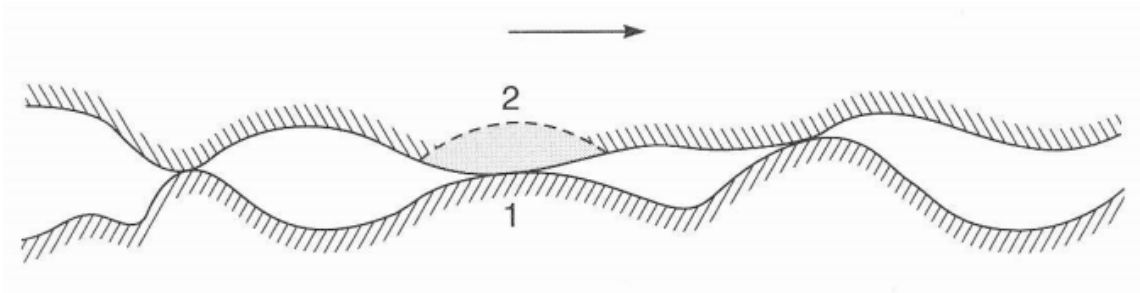

Figure 7. *Schematic presentation of adhesive wear showing two possibilities for fracture during shearing of an interface. Path 1: fracture occurs at the interface. Path 2: fracture occurs within one of the two bodies. [14]*

Based on experimental data obtained on numerous unlubricated material pairs, written “laws” have been formulated for the adhesive wear. The amount of wear is generally directly proportional to the applied load W and sliding distance L and inversely proportional to the hardness H of the surface being worn. The nondimensional wear coefficient k_{ad} describing the relation between the worn volume and the normal force sliding distance and surface hardness is dependent on the materials in contact. The Archard equation [20] is presented in equation (2) and it describes the volume of material being worn away. It was first developed by Holm [19] for sliding electrical contacts and later Archard [20] presented the theoretical basis for the expression covering more generally the typical adhesive sliding conditions. This wear equation shows that the wear is directly

proportional to load and to the sliding distance but that it is independent on the apparent contact area and sliding velocity.

$$V = \frac{k_{ad} W L}{H} \tag{2}$$

The hardness of the wearing surface should be used in the calculation of k for either surface in equation (2). The value of k_{ad} ranges typically from 10^{-8} to 10^{-4} for mild wear and from 10^{-4} to 10^{-2} for severe wear for most material combinations. The value of k depends also on operating conditions. The Archard wear equation suggests for a system with constant k_{ad} that the wear rate is directly proportional to load on the contact but inversely proportional to the surface hardness of the wearing material. [21] Consequently it can be written as:

$$\kappa = \frac{V}{WL} \tag{3}$$

where: κ is the dimensional specific wear rate, SWR.

Rabinowicz [22] has stated that the metallurgical compatibility indicates the tendency of the sliding metals to adhere strongly to each other. Metallurgical compatibility means mainly the degree of solid solubility between two metals. Increasing degree of incompatibility lowers the value of the wear coefficients and the coefficient of friction and it also reduces wear. The lubrication between the sliding surfaces also influences the amount of wear.

According to Rabinowicz [22] hexagonal close packed (HCP) metals exhibit lower friction coefficients and wear rates than cubic metals. This is due to the limited number of slip planes in hexagonal metals. Tangential shear under compression at the contact interface with strong adhesive bonding generates slip inside the material along the slip planes. [14, 17]

2.6.2 Abrasive wear

Abrasive wear occurs when the asperities of a rough, hard surface or hard particles slide on a softer surface and damage the interface by plastic deformation or fracture. As Figure 8 shows, there are two general situations for abrasive wear. Two-body abrasion means that one surface is the harder of the two rubbing surfaces. In the second case, the hard surface is a third body, generally a small particle of abrasive. The abrasive particle is hard enough to abrade either one or both of the mating surfaces. It is common that in the beginning the wear mechanism is adhesive. It produces wear particles that get between the interfaces; this leads to the three-body abrasive wear. [14]

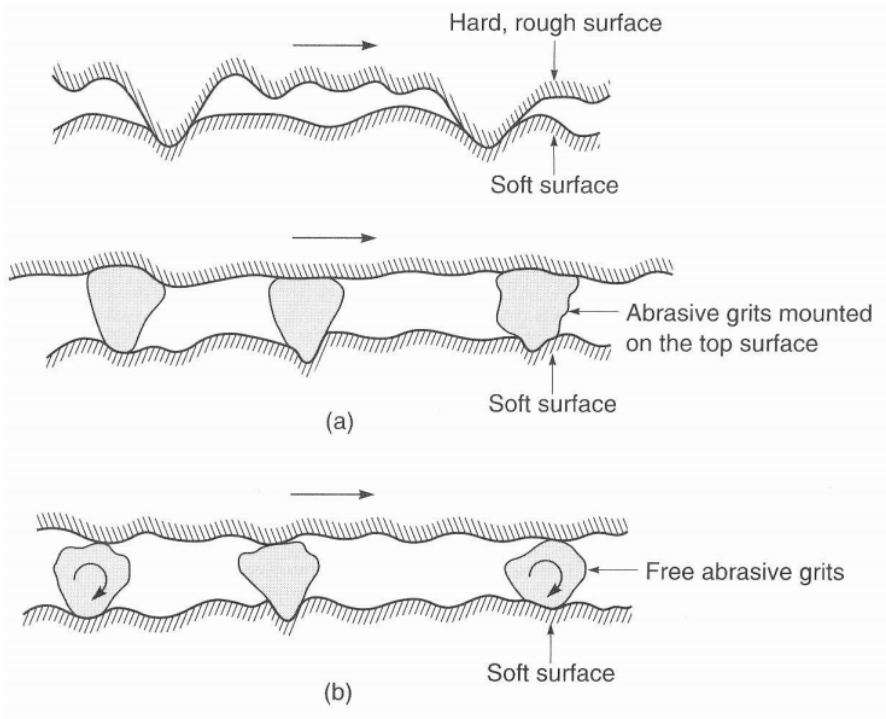

Figure 8. *Schematic presentation of two general abrasive wear situations. (a) A rough, hard surface or a surface mounted with abrasive grits is sliding on a softer surface. (b) Free abrasive grits caught between the surfaces where at least one of the surfaces is softer than the abrasive grits. [14]*

Parallel grooves are generally found on the wear surfaces after sliding even in the case of sliding contact between smooth surfaces of the same ductile material. The hard abrasive asperities are formed on the mating surface due to the work hardening, phase transformations and due to the third-body formation at the contact interface during sliding. An equation similar to equation (2) is found to cover a wide range of abrasive situations. The only difference is in the wear coefficient k_{ab}, which in this case includes the geometry of the asperities and the probability that the asperities rather cut than plough. The value of k_{ab} typically ranges from 10^{-6} to 10^{-1}. The rate of abrasive wear is often very high, two or three orders of magnitude higher than in the adhesive wear. [14]

Abrasive wear may assume three different modes: microcutting, wedge forming and ploughing as shown in Figure 9. Wear particles are formed differently depending on these three modes. In the cutting mode, long and curled ribbon-like wear particles are formed. Low friction assists in this wear mode. This process results generally in a significant removal of material. A wedge-like wear particle is formed at the tip of the grooving asperity in the wedge-forming mode. In this case, only some of the material is displaced to the sides. High friction or strong adhesion assist in this wear mode. In the ploughing (also called ridge formation) mode, material is displaced from a groove to the sides without the removal of material. However, when the surface has been ploughed several times, material removal occurs by low-cycle fatigue mechanism. After repeated loading and unloading cycles ridges which are formed along the sides of the grooves become flattened and eventually fractured. [14, 17]

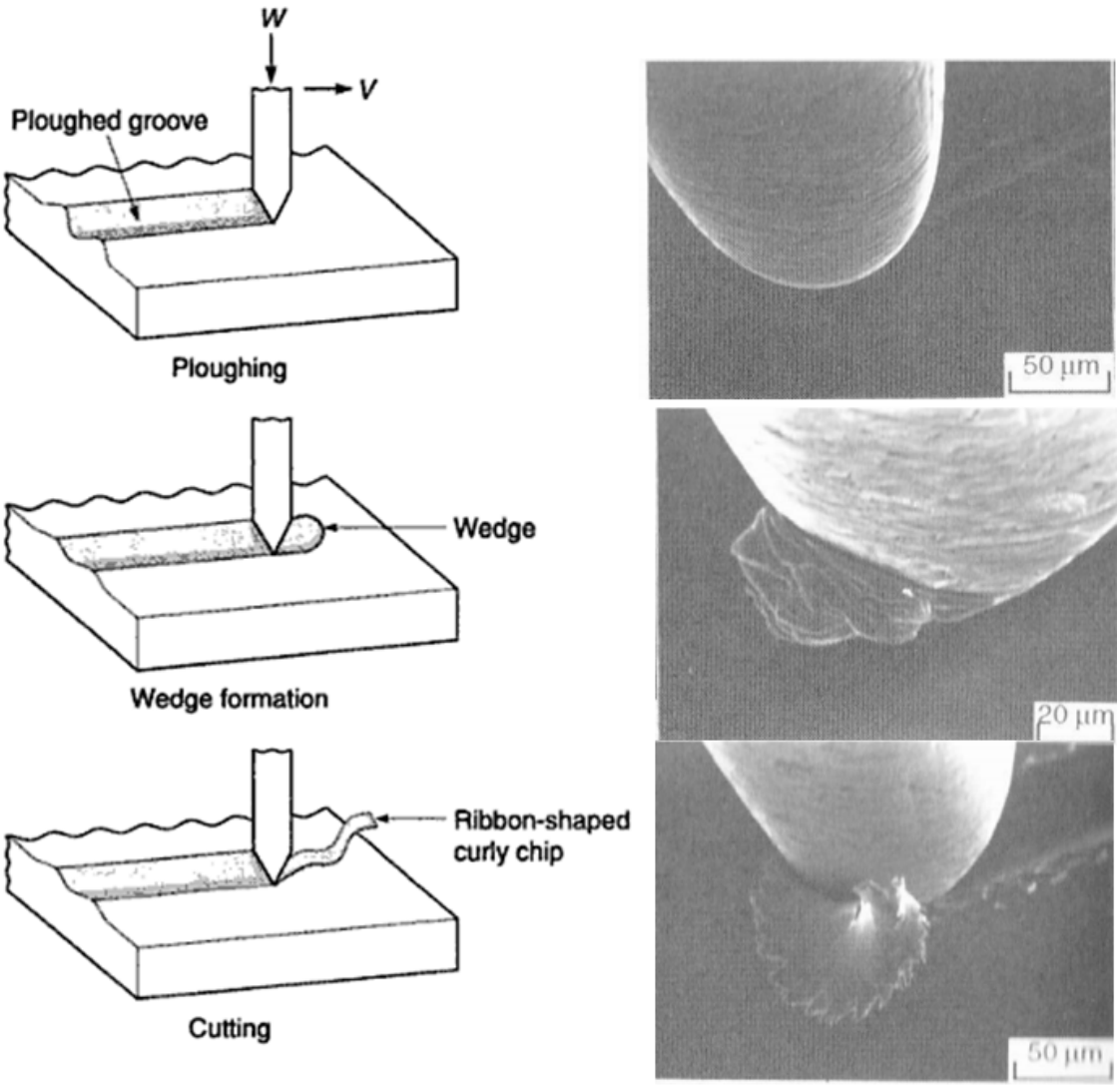

Figure 9. *Schematic presentation of abrasive wear processes as a result of plastic deformation by three deformation modes. Images on the right are SEM micrographs obtained during the wear of unlubricated brass by steel pin. [14]*

In all of these wear modes grooves are formed as the result of wear particle generation and plastic flow of material to form ridges on both sides of the groove. During wear, some blunting of the hard asperities or abrasive particles occurs, thus reducing the wear rate. However, an increase in wear rate is possible when brittle abrasive particles are fractured and the edges of the particle are resharpened.

Hardness plays a key role in the abrasive wear resistance. It has been verified that a metal surface strain hardens by plastic flow during abrasion to a maximum value and that this maximum value of hardness is important for abrasion resistance. On the other hand, when a material is hardened, it usually becomes less ductile. Brittle materials tend to produce larger particles, resulting in high wear rates. [14, 17, 18]

2.6.3 Fatigue wear

Repeated cycles of contact are necessary in the generation of wear particles by fatigue wear. The repeated loading and unloading cycles to which the materials are exposed may induce the formation of subsurface or surface cracks, which eventually will result in the fracture of the surface with the formation of large fragments, leaving large pits in the surface. Cracks are nucleated at and below the surface as the deformation goes on. Further loading and deforming causes cracks and pre-existing voids to extend and propagate. After a critical number of contacts an asperity fails due to fatigue, producing a wear particle. In a sliding contact the friction is generally high as compared to the rolling contact. This means that the maximum shear stress occurs at the surface and leads to surface fatigue. The amount of material removed by fatigue wear is not a useful parameter. For example, the time after which the fatigue failure occurs is much more relevant. Fatigue wear does not necessarily require direct physical contact between two surfaces. Stresses can be transmitted also through the lubricating film. [14, 17]

Suh [23] developed a delamination theory of wear in 1974. The theory has been popular ever since due to the frequent observation of wear debris in the form of flakes. Delamination wear occurs as a result of repeated sliding and is a mechanism contributing to the loss of metal. The mechanisms of delamination wear involve the initiation of subsurface cracks which propagate parallel to the surface and lead to the detachment of flakes. These cracks are thought to initiate at voids and vacancies developed from dislocation pile-ups below the surface layer. After reaching the critical length the cracks shear to the surface. The delamination theory of wear is applicable only to the cases where the sliding speed is low and the temperature rise at the contacting surface is so low that diffusion and phase transformations are not involved in the wear process. A schematic presentation of the formation of delamination wear is shown in Figure 10. [18, 24]

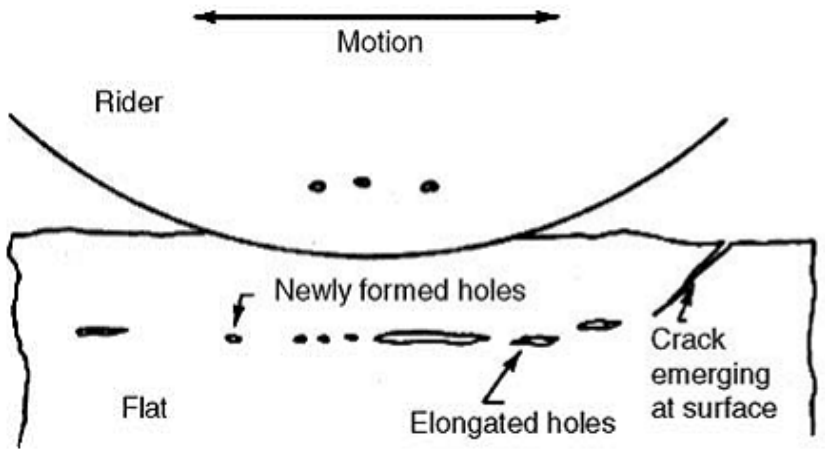

Figure 10. *A schematic presentation of the formation of delamination wear. [24]*

2.6.4 Corrosive wear

Corrosive wear or chemical wear occurs when the sliding takes place in corrosive liquids or gases. In air atmosphere, the most dominant corrosive medium is oxygen. Therefore wear in the air atmosphere is usually called oxidative wear. When there is no sliding between surfaces, the chemical products of the corrosion may form a thin, protective film. The film tends to slow down the corrosion. The sliding action, however wears the chemical film away and allows the chemical attack to continue. The chemical wear requires both chemical reaction and rubbing. Corrosive wear is presented in Figure 11. The rate of chemical reaction increases by the frictional heat produced at the contact point of sliding surfaces. This means that the reactions which normally occur only at high temperatures may occur at moderate or even ambient temperatures during sliding. [14, 17]

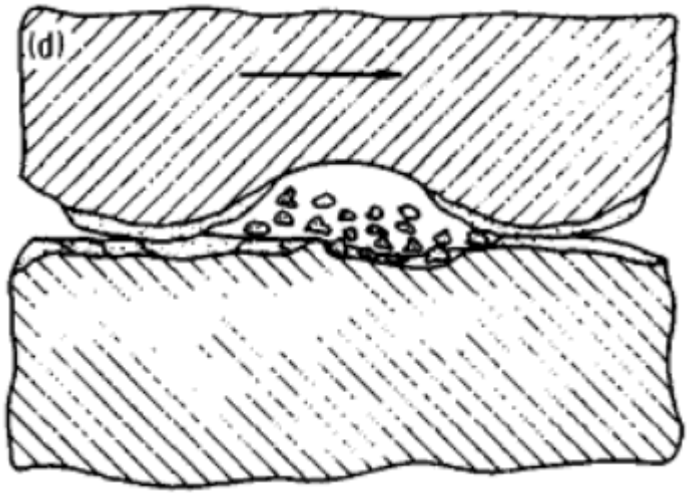

Figure 11. *The cracking of reaction films in corrosive wear due to the sliding motion. [16]*

2.7 Variables influencing wear

The wear process has a large number of variables and by understanding how they influence the friction and wear, the process can be controlled and evaluated. Variables influencing wear are combined to the following categories which are considered as significant: materials and the operational, geometric and environmental factors. Due to the large amount of variables, only the important ones from each category are presented in the following. [25]

The composition, properties and microstructure of the materials determine their wear rates under different operating conditions. The properties of particular significance are hardness, impact strength, toughness, modulus of elasticity, corrosion resistance and fatigue resistance. As mentioned previously, the solid solubility of materials has also an influence on wear rate. In general, the wear of alloys tends to be lower than that for pure components. Based on the chemical composition and processing, a variety of micro-

structures and physical properties of ductile iron can be obtained. The wear resistance of different microstructures is summarized in Figure 12. [16]

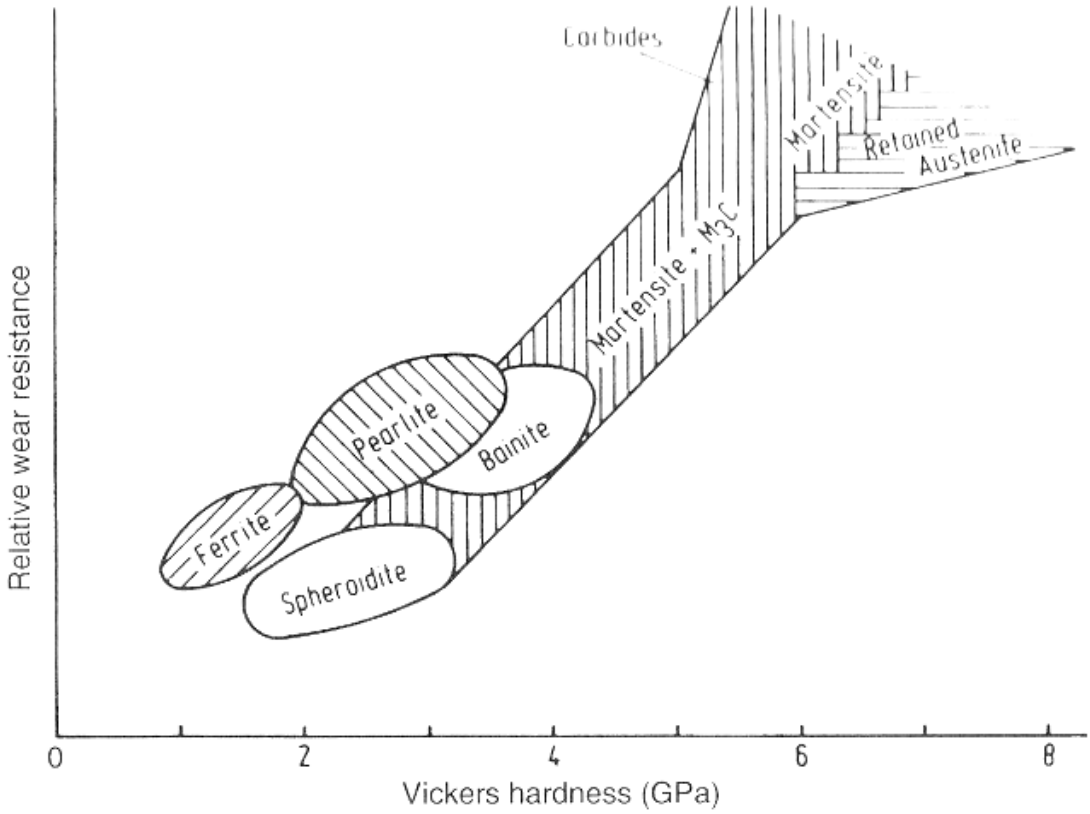

Figure 12. *Relative wear resistance of different microstructures of cast iron matrix as a function of hardness. [16]*

The operational variables which significantly influence the wear are normal load, sliding velocity, time and temperature. As the load is increased, the wear rate will increase regardless of the amount of lubrication. An increase in normal load also increases the frictional heat. Generally the increase in the sliding velocity has the same effect as load. However, a decreasing wear rate may occur at higher velocities, because there is less time available to develop a full wear particle. In the initial stage the wear rate is high and decreases to a constant value when the surface contact area increases with time. The wear rate increases after operating for a definite period of time. This transition can be attributed to a number of causes such as a change in the type of wear, an increase of the surface temperature to a critical value or lubricant contamination. [25]

Geometrical variables are those defining the geometrical contacts between the solids and between different materials. They are typically surface roughness, surface topography, particle size and shape. The changes in the contact characteristics which occur during the wear process can be observed and explained on macrolevel, microlevel and nanolevel. [25]

Environmental variables are typically the amount of lubrication, contamination, ambient temperature and atmosphere. For instance, changes in temperature influence the

wear rate by modifying the surface properties of materials and the properties of lubricant. Increasing humidity usually makes the wear process faster. [18, 25]

2.8 Wear maps

Wear is a complex function of the system which includes material properties, operating conditions, contact geometry and environment. The dependence of wear on such a large number of variables has been a significant barrier for achieving a comprehensive representation of wear. Comparison of wear test results obtained with the same material is difficult due to the variations in materials themselves. Therefore, there is a strong need to develop a methodology for defining and measuring the wear of a material in definitive terms. [18]

A wear map is a diagram which shows the regimes of different wear mechanisms. In a wear map the regimes are shown as a function of two variables set along the two coordinate axes. This is, of course, a simplified and approximate way to present wear mechanism regimes, because only two variables are considered while the others are kept constant. The wear map gives a good indication how the wear mechanisms change as a function of wear variables if the two selected variables are those having the dominating influence on wear under the studied contact conditions. [18, 26]

Lim and Ashby [26] constructed wear maps using the pin-on-disc (steel on steel) wear test data measured under dry sliding conditions presented in the literature. As an example, the wear regime map for steel sliding on steel in air at room temperature is shown in Figure 13.

It shows how the dominating wear mechanism changes with the two main operating variables, load and sliding speed, given as normalised pressure and normalised velocity. Normalized pressure is the nominal pressure divided by the surface hardness and normalized sliding speed is the sliding velocity divided by the velocity of heat flow. The geometrical and environmental variables are considered to be constant and to correspond to the pin-on-disk device in laboratory environment. The material variables are also considered to be constant and to correspond to the steel against steel contact. The general form of the map would be similar for the sliding of most unlubricated metals in air.

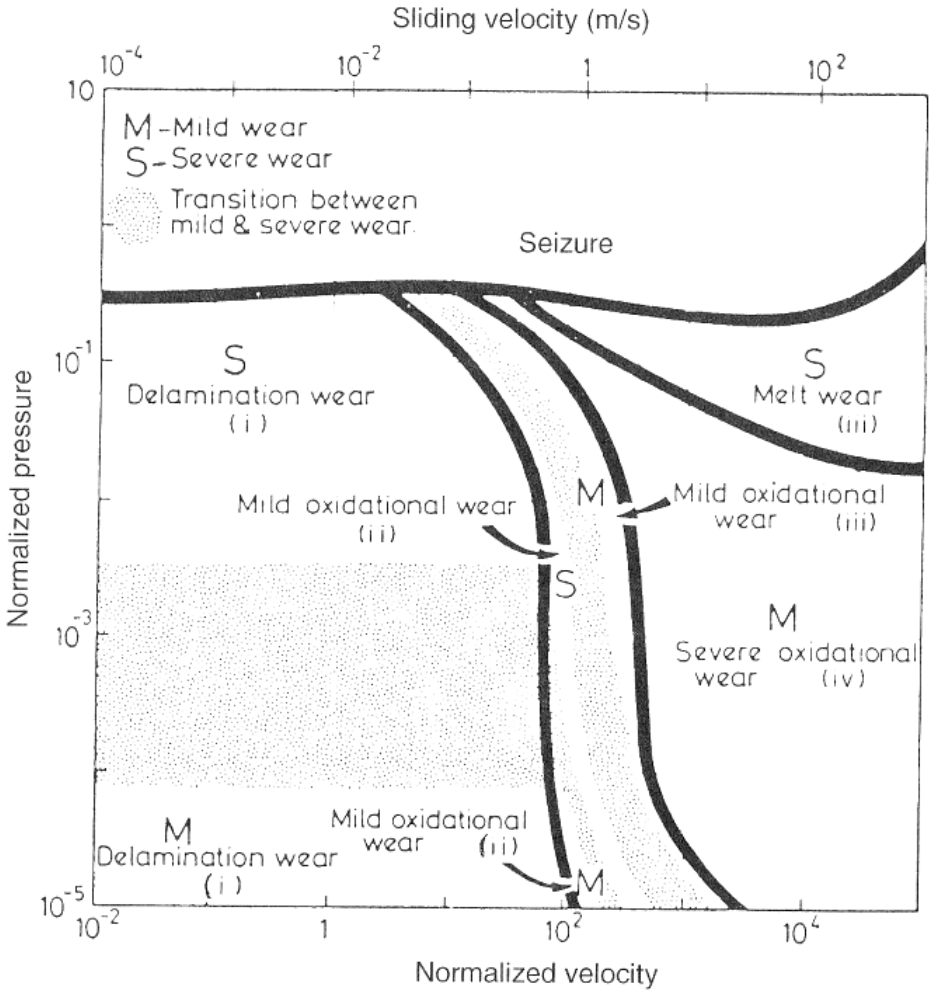

Figure 13. *Wear regime map for dry sliding in steel on steel pair in air atmosphere at room temperature when using the pin-on-disc configuration. [14]*

Lim and Ashby have identified the following wear mechanisms in their wear map: seizure, melt wear, oxidational wear and plasticity-dominated wear. These wear mechanisms are combinations of some of the basic wear mechanisms described earlier. Seizure combines typically adhesion and abrasion, melt wear is mainly severe adhesion, oxidational wear combines adhesion and chemical wear while plasticity-dominated wear combines adhesion and surface fatigue. The transition from the wear regime of mild wear to another representing severe wear may be due to the load-dependent rupture of thin oxide surface films or the sliding velocity-dependent formation of hard martensitic surface layers. The transition from severe to mild wear during the run-in process may be due to the sliding distance-dependent martensite formation at higher sliding velocities, or to a combination of work hardening, surface oxide films and the smoothening of original surface roughness at lower velocities [26, 27].

2.9 Wear of cast irons

The dependence of wear on both material properties and environment prevents the use of a universal wear test for comparing and evaluating the wear behaviour of different materials under different wear conditions. This has led to the situation where the wear resistance is evaluated with many test methods, with each test applying to specific conditions. Therefore, the discussion of wear resistance of ductile irons is here limited to general level. As the thesis is dealing with continuous sliding wear of different ductile iron grades, example results from similar types of wear tests found in the literature review are collected to the end of this chapter.

Cast irons are considered to be ideal materials for a wide range of wear applications, especially for frictional sliding wear under both dry and lubricated conditions. Under dry sliding conditions the graphite particles in cast iron lubricate the mating surfaces, reducing friction and heating at the contact points. The graphite particles on the wear surfaces can also act as reservoirs for oil under lubricated sliding conditions. Microstructure mainly determines the wear resistance of ductile irons. Pearlitic structure exhibits good wear resistance under conditions where both friction and moderate abrasion occur. Improvements in abrasive wear resistance can be obtained through alloying and heat treatment by producing a harder martensitic or ausferritic matrix. [3]

ADI has a superior abrasion resistance and low sensitivity of abrasion resistance to bulk hardness. This is resulting from the strain-induced transformation of stabilized austenite which occurs when the surface is subjected to deformation. The transformation increases surface hardness significantly as shown in Graph 1. The surface layers need sufficient deformation to transform into martensite. Martensite transformation can also be due to work hardening of austenite. The amount of stabilized austenite increases along with the austempering temperature. The bulk hardness of ADI, on the other hand, is reduced by the austempering temperature. This means that the abrasion resistance and related mechanical properties of an ADI component can be optimized by varying the austempering conditions. For a combination of high toughness and abrasion resistance the austempering temperature in the range of 350 - 375° C should be adequate. When high strength and abrasion resistance are required, the austempering temperature of 260° C will give the best results. [3]

There are three types of wear resistant alloy irons available for demanding wear conditions. The first is formed by unalloyed and low alloy grades of white iron having a structure of massive carbides in a pearlitic matrix. These alloys are extremely brittle. Ni- hard irons contain nickel to increase hardenability and to ensure that the austenite transforms to martensite after heat treatment. High Cr-Mo white irons combine abrasion resistance with toughness. Hardenability is increased by Mo. It allows heavy section castings to be produced with a martensitic structure either with or without heat treatment. Some components may be cast as pearlitic to aid machining and then they are heat treated afterwards. These types of cast irons are used in mineral processing industries in applications such as grinding balls and hammers for rock crushers. [28]

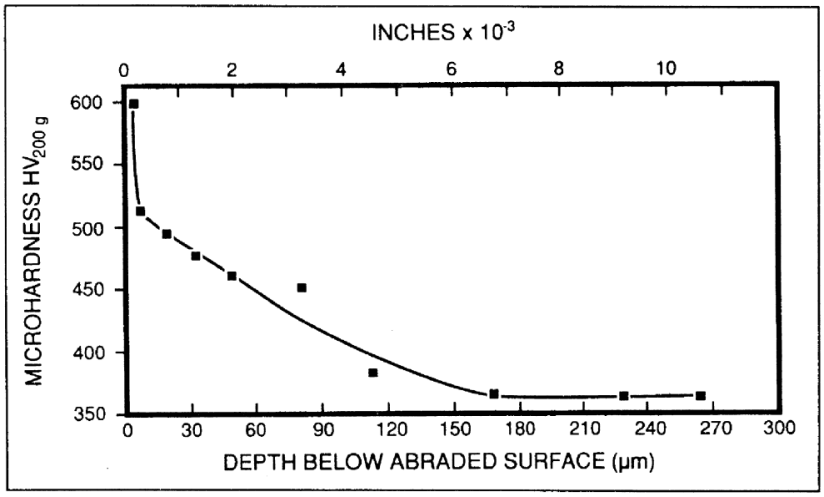

Graph 1. *Microhardness profile of an abraded ADI sample. [3]*

Islam et al. [29] have studied the wear behaviour of as-cast and heat treated ductile iron samples under dry sliding conditions using a pin-on-disc type apparatus. The wear tests were carried out at a linear sliding speed of 0.88 m/s under a constant load of 1.5 kg. The as-cast ductile iron had pearlitic matrix, while the heat treated ductile iron had a matrix of tempered martensite. The studied materials were used as the pin and grey cast iron was used as the disc. They found out that the high hardness of martensitic matrix in the heat treated samples resulted in lower wear rates as compared with the as-cast samples. The wear rate measured after 9500 m of sliding was about three times higher with the as-cast ductile iron. They also discovered differences in wear mechanisms. The heat treated samples were worn mainly by an abrasive mechanism, whereas the as-cast samples underwent a combination of adhesive wear and surface fatigue or delamination mechanisms. Generally the wear is considered as mild, oxidative type under these experimental conditions. The hardness near the surface of the heat treated samples was found to decrease during the testing due to the tempering caused by frictional heating. On the contrary, the as-cast ductile iron showed a slight increase in microhardness due to the strain hardening effect. However, this was not enough to cause any subsequent decrease in the wear rate of the as-cast ductile iron. [29]

The friction and wear characteristics of ductile iron under severe sliding conditions at high sliding speed and high contact pressure have been experimentally studied by Hirasata et al. [30]. All the tests were carried out with a pin-on-disc type test rig under conditions of room temperature and dry friction. Ductile iron FCD 800 was used as pin material and mild steel SS 400 as disc material. The results of the wear tests by Hirasata et al. [30] showed that the wear rate of ductile iron depends on the contact pressure and the sliding speed. The rate is proportional to the contact pressure in all wear regions increases due to the increment of sliding speed in the first two wear regions but goes to the contrary direction in the third wear region. They also found that the coefficient of friction decreases with the increment of sliding speed and is almost independent on the contact pressure. [30]

Lerner [31] has been studying the wear resistance of different grades of ductile iron while exploring potential applications of ductile iron as a bearing material against steel in steel shafts. Rotating sliding tests were carried out with lubricant, under the load of 7.5 MPa and at the rotating speed of 0.31 m/s. Test duration was 20 hours and the wear resistance was evaluated using the weight loss. Results indicated that alloying with silicon had a positive influence on ductile iron wear resistance, but it was recommended only for static loading conditions because it drastically reduced impact wear resistance. Silicon content in the test materials containing silicon was 4 % and 4.7 %. Alloying with 1 % copper also improved wear resistance and did not cause brittleness. [31]

Lerner et al. [32] have been studying the wear resistance of austempered ductile iron under adhesive dry sliding. The test conditions were similar to Lerner's [31] previous tests, except that no lubricant was used in this study. The shaft was made from quenched 1045 steel. Unalloyed pearlitic ductile iron grade 100-70-03 (equivalent to EN-GJS-700-2) was used as the reference material. Table 7 shows the heat treatments, matrix microstructure and hardness of tested materials. The measured wear rate and friction coefficient of the tested materials in dry sliding tests are presented in Table 8. The wear resistance of pearlitic ductile iron grade GJS-700-2 was improved by alloying with 4 to 4.7 % silicon and with 4 % silicon + 0.4 % phosphorus. In the dry sliding wear tests the ADI iron, grade 175/125/4 (equivalent to EN-GJS-1200-3), was found to have nearly four times higher wear resistance than the pearlitic reference ductile iron. [32]

Table 7. *The materials tested in ref. [32] under wear conditions of rotating dry sliding.*

Index	Material	Heat treatment	Metallic matrix(a)/hardness
1	DI, grade 100-70-03	Normalized	Pearlitic, 3-7% ferrite, 255-271 HB
2	DI (4% Si)	Normalized	Pearlitic, 2-5% ferrite, 265-271 HB
3	DI (0.7% Mo)	Normalized	Martensitic, 10% acicular, 453 HB
4	DI (0.4% Si, 0.4% P)	Normalized	Pearlitic, phosphide eutectic, 273-281 HB
5	DI (4.7% Si)	Normalized	Pearlitic, 10% ferrite, 302-311 HB
6	ADI, grade 175/125/4 (alloyed with Mo and Ni)	Austenitized at 900 °C (1650 °F) for 2 h, austempered at 300 °C (570 °F) for 2 h	Ausferrite, 42-44 HRC
7	Nitrided DI	Heated in a dissociated ammonia atmosphere for 16 h at 550-560 °C (1020-1040 °F)	0.25 mm (0.01 in.) nitrided layer, including 0.08 mm (0.003 in.) with nitride particles (550-650 HV) and a nitrogen-rich austenitic underlayer (300-350 HV)
8	Quenched DI	Quenched in water, tempered for 1 h at 220-240 °C (430-465 °F), cooled in air	Martensitic, 48-50 HRC
9	Aluminum bronze (9% Al, 4% Fe)	As cast	123-127 HB
10	Leaded-tin bronze (4.5% Pb)	As cast	115-121 HB

(a) Graphite nodularity in all DI samples was not less than 80%.

Table 8. *The wear rate and coefficient of friction for materials tested in ref. [32] against hardened 1045 steel rings in dry sliding tests.*

		Wear rate, g/h		Wear factor		
Index	**Material**	**Test material**	**Steel shaft**	**Test material**	**Steel shaft**	**Friction coefficient**
1	PDI, grade 100-70-03	0.2940	0.1000	1.0	1.0	0.472
2	DI (4% Si)	0.2890	0.0820	0.98	0.82	0.478
3	DI (4.7% Si)	0.2560	0.0460	0.87	0.76	0.497
4	DI (4% Si, 0.4% P)	0.1740	0.0360	0.59	0.66	0.484
5	Nitrided DI	0.1223	0.0573	0.416	0.58	0.524
6	DI (0.7% Mo)	0.091	0.0589	0.309	0.57	0.482
7	ADI, grade 175/25/4	0.0788	0.0440	0.268	0.44	0.436
8	Quenched DI	0.061	0.0420	0.207	0.42	0.437
9	Aluminum bronze (9% Al, 4% Fe)	1.082	+ (increment)	3.68	…	0.457
10	Leaded-tin bronze (5% Sn, 4.5% Pb)	0.9594	+ (increment)	3.22	…	0.331

The influence of nodule count on the sliding wear behaviour of a ferritic-pearlitic ductile iron has been studied by Abedi et al. [33]. They carried out wear tests using pin-on-disc type apparatus based on ASTM-G99 standard under dry sliding conditions, with the nodule count varying between 150 and 450 nod/mm^2. The results showed that the sliding wear process in ductile iron consisted of three wear mechanisms (oxidational, adhesive and delamination) depending on the nodule count and applied load. They also found that at the lower applied load, the samples with high nodule count showed lower wear rate than those having the low nodule count. At higher loads the wear resistance was reduced with increasing nodule count. [33]

Dommarco et al. have been reported that increasing nodule count could have a negative influence on the abrasion resistance of ductile irons. Due to the low mechanical resistance of graphite, the penetration depth suddenly increases when an abrasive particle reaches the leading edge of the graphite nodules. Usually this means that the exit edge of the nodule is worn away in the form of a comet tail. [34, 35]

According to Zimba [36], graphite acts as a solid lubricant during the initial stage of wear by reducing the friction between contact surfaces. However, this kind of behaviour of graphite nodules may not be observed when applying high loads and long sliding distances. The reason is that under these conditions the temperature of the contact surfaces increases and therefore the graphite may loose its efficiency as a lubricant. [36]

Ahmadabadi et al. [37] have reported that the wear of austempered ductile iron was due to the subsurface fatigue, with cracks readily nucleated from the plastically deformed nodular graphite. They observed severe plastic deformation and cracks initiating at and propagating from the nodular graphite. In their studies the delamination seemed to be the main wear mechanism as observed from the subsurface micrographs of the worn samples. [37]

3 AIM OF THE WORK

The aim of this Master of Science thesis is to study the wear of different ductile iron grades against steel in continuous sliding motion. The main goal of the work is to get comparable information on the wear resistance and wear behavior of selected ductile irons. Since the thesis is a part of the DEMAPP – HICON project, the results are also discussed from the viewpoint of the project. DEMAPP (Demanding Applications) program develops novel breakthrough materials with improved performance for applications under demanding operational and service conditions. HICON (High Friction Low Wear Contacts) aims to find solutions for increasing friction and simultaneously decreasing the wear. The applications studied in HICON have a definite amount of sliding wear and they currently use GJS-700-2 ductile iron. This is the reason why GJS-700-2 is used as the reference material in the discussion of the results. It is clear that the wear rate of the counterpart is desired to be minimal. In this case it means the steel wire which is used as the pin material.

The total number of different ductile iron grades used in the tests is 10 and all materials are based on EN- standard. Novel high silicon and heat treated grades are also included. The tests are run with a pin-on-disc type tribotester using special sample geometry. The disc material is machined from tensile test bars of the ductile iron and the pin material is steel wire used in steel ropes. The tests are carried out with and without lubrication. After the tests worn samples are studied with optical microscope to evaluate the amount of wear. The original plan contained also the evaluation of operating wear mechanisms with scanning electron microscope but this was left out due to the tight time schedule of the thesis.

The experimental test procedures are presented in the following chapter. The experimental work consists of sample preparation and sample holder design, preliminary and actual wear tests and sample analyzing. The methods for converting the data from the wear tests to better understandable and comparable forms are also explained.

4 EXPERIMENTAL WORK

4.1 Sample preparation

There are two kinds of samples needed in the pin-on-disc wear test, a disc and a pin. In this case the disc material is cast iron and the studied steel wire is used as a pin. To speed up the beginning of the experimental work, discs were decided to be machined from the ends of the tensile test bars. A majority of the tensile test bars are cast in Componenta Karkkila foundry as a part of normal quality control. The tensile bars are cast separately in molds made from core sand. Tensile bar mold is presented in Figure 14. Casting tensile bars separately helps them to be flawless. Before the disc sample is machined from the end of the tensile bar, tensile and hardness tests are carried out. Chemical analysis is also available for each bar. All the discs and their properties are listed in Appendix 1. The known mechanical properties and chemical analysis are an other good reason why the discs are made from the bars.

Figure 14. *The mold of tensile test bar made from core sand and the end of the tensile test bar.*

The tensile tests were completed according to the EN 10002-1 standard. The ductile iron standard EN 1563 defined the test piece. The end of the tensile test bar where the discs were machined is shown in Figure 1. The diameter of the bar end is 25 mm; based on that the diameter of the disc was decided to be 23 mm. The height of the disc is 7

mm and there is a 6 mm diameter hole in the middle of the disc. Hole in the middle only makes the lapping process easier. With these dimensions two discs could be machined from one test bar. All samples were carved with an identification number on the side so that they did not get mixed up in the lapping process. The discs needed to be lapped to ensure sufficient parallelism of the surfaces. The other side of the discs was also polished to obtain the best possible surface roughness. The lapping and polishing was done by Tiivistetekniikka Ltd. After lapping and polishing the discs were ready for wear tests. A complete and already worn disc is shown in Figure 15.

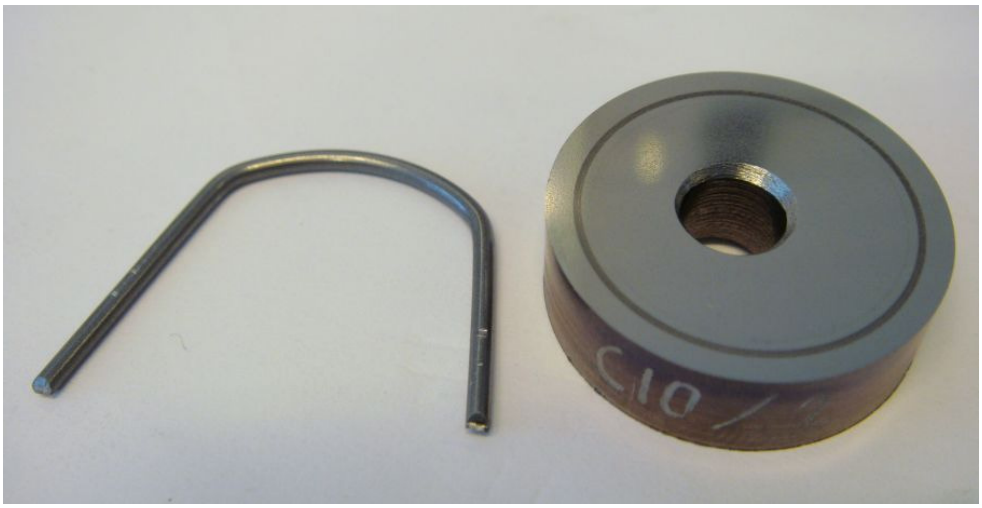

Figure 15. *Pre-bent steel wire and cast iron disc after a wear test.*

The size of the disc set also limits to the pin size. As the thesis is a part of the Demapp project, it was a coherent decision to use a steel wire as the pin material. Steel wire is used in steel ropes which are utilized in elevators and cranes. The steel wire had a diameter of 1.4 mm and it was produced according to the standards EN 10264-1 and EN 10264-2 [38, 39]. The tensile strength of the wire was 1570 N/mm^2 and it was not coated.

The hardness of the pin was measured in the laboratory of Tampere University of Technology. The scale used in the measurements was HV0.3, which means Vickers hardness with load of 3 N. The test results revealed that the harness of the pin was 435 ± 3 HV when measured parallel to the pin and 453 ± 6 HV when measured perpendicular to the pin. Converted to Brinell hardness, used with the discs, hardness of the pin was approximately 410 or 430 HB depending on orientation of the measurements.

Steel wire itself does not need so much preparation as the disc. The wire needs to be pre-bent to ensure that the radius of the curve is equal on desired length. Pre-bending also made the wire assembly faster. Bending was carried out with a special jig, designed and manufactured especially for the thesis. The radius of the curve was 9.5 mm and this radius could be produced with the jig that had a groove with the same radius. The pre-bent steel wire can be seen in Figure 15.

4.2 Test apparatus

4.2.1 Pin-On-Disc device

All the tests in the study were performed with a pin-on-disc machine, Figure 16, at VTT Laboratory of Tribology in Otaniemi. Pin-On-disc apparatus is a tribometer that measures friction and wear in a sliding motion. This test apparatus is probably the most commonly used for tribological applications of materials. Steel wire pin and cast iron disc were the samples used in the study. Due to the special sample geometry sample holder for the pin was designed especially for this experiment. The sample holders are presented in the next chapter. The pin was held stationary and perpendicular to the disc which rotated counterclockwise. The pin was pressed with a defined force against the rotating disc. Friction force and consequent friction coefficient were measured during the test with a load cell. The spinning speed was monitored with two meters. Wear rate of the tested material was defined as volume loss per sliding distance. After the test the surface of the disc was analyzed with optical profilometer for the volume loss. An optical microscope was utilized to evaluate the wear characteristics of the pin.

Figure 16. *The pin-on-disc test apparatus in VTT, Otaniemi.*

Although the sample geometry was different from the commonly used the tests were still carried out according to the ASTM G99-95a standard [40]. Standard is mainly a directional guide for determining the wear of materials during continuous sliding using a pin-on-disc apparatus. For instance the standard defines the following things:

- Wear results are reported as volume loss in cubic millimeters for both two specimens separately.
- Wear apparatus should have a revolution counter or its equivalent.
- Instruments to obtain linear measures of wear should have a sensitivity of 2.5 µm or better.

- Surface finish. A ground surface roughness of 0.8 µm arithmetic average or less is usually recommended.
- Interruptions or restarts during the test are not allowed.
- Specimens have to be cleaned and dried prior to testing and measuring.
- The disc has to be fixed perpendicular (±1°) to the axis of the revolution and the pin has to be perpendicular (±1°) to disc surface.

A few examples where the standard does not give definitions:

- How the amount of wear is determined. The standard states that linear measures of wear are more frequently used in practice because the mass loss is often too small to be measured precisely.
- Test conditions because they are depending on the purpose of the test.
- Which one is spinning, the pin or the disc. All that matters is that the wear track on the disk is a circle.
- The size of the specimens.

4.2.2 Sample holders

As mentioned earlier, the pin holder was designed especially for the thesis. Figure 17 shows the pin holder with the steel wire placed on it. The pin holder consist of four parts: base part, wheel part and two side blocks. All parts are made from steel and they were designed for easy manufacturing. The pin holder was made in Protoshop Oy according to the drawings shown in Appendix 2. The dimensions of the base part were adjusted so that the pin holder fitted to the pin-on-disc machine at VTT. The wheel part had a groove for the wire on the top. This groove guaranteed that the wire stayed straight during the test. The bottom of the groove that goes along the side of the wheel had the same radius as the pre-bent wire. The wire was tightened against the wheel part with two side blocks. Inside of both blocks were short tightening screws and they were used to lock the wire to the block.

The disc holder already existed and it has been used for tribological testing in different projects. A small modification was needed to the disc holder because the center slot was too big for the disc. The Protoshop Oy also delivered six aluminum rings with different inner diameters to fit the discs to the holder. The disc was placed in middle of the slot surrounded by the matching aluminum ring and then tightened up with two screws. The holder itself was attached to the pin-on-disc machine with four hexagon screws. The disc holder with attached disc sample is presented in Figure 18.

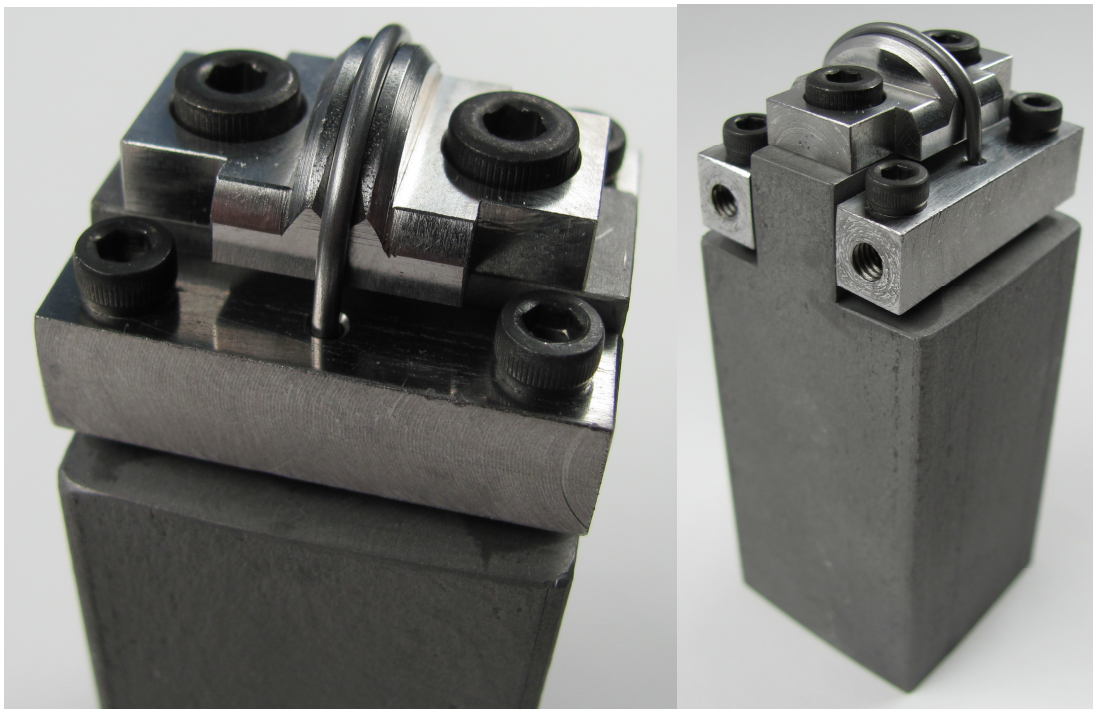

Figure 17. *The pin holder with the steel wire pin*

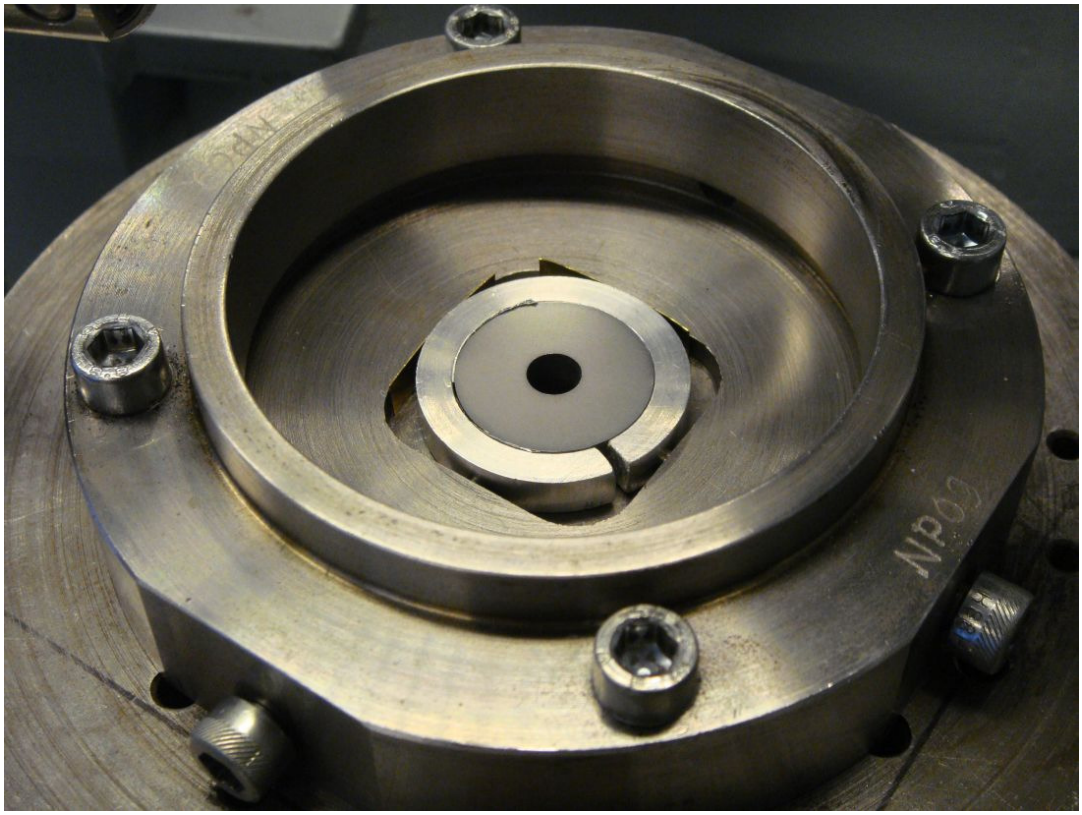

Figure 18. *The disc holder with attached sample disc.*

4.3 Pre-tests

Pre-tests were carried out to find the proper test parameters for these materials and for this type of sample geometry. First three pre-tests were done with same parameters be-

sides the different normal force. Based on these tests the load of 5N was decided to be used in the actual tests. Sliding track was increased to the diameter of 20mm from the 16mm that was used in the pre-tests. Sliding speed was also doubled by increasing the amount of revolutions per minute to 95 RPM instead of 60 RPM, which was used in the pre-tests. Sliding speed was 0.1 m/s and to reach the total sliding distance of 250 meters, test duration was decided to be decreased to 42 minutes. Materials in the pre-tests were taken from both ends of the hardness scale of all irons included in the thesis. The softest, GJS-400-15 and the hardest, GJS-1200-3 were used to ensure that with the hardest material pin does not wear too much and also to ensure that the wear track in the disc is big enough. The pin was not allowed to penetrate too deep into the disc and this was the reason why GJS-400-15 was used as a pre-test material. The wear tracks in the pre-test discs were only visually inspected instead of using a profilogram. One lubricated test was carried out with the same parameters, only increasing test duration to 8 hours and sliding distance to 2.8 km. Sliding distance was still increased to 4.3 km in actual lubricated tests. This means that the test duration was 12 hours.

4.4 Test procedures

All wear tests in the thesis were carried out with similar test procedures. In the beginning of the tests the pin-on-disc apparatus was calibrated. The calibration ensured that the friction force was measured with sufficient preciseness. The lever where the pin holder was attached, was balanced at definite intervals. Balancing was carried out by adjusting the counter weights. The samples were cleaned immediately prior to each test with ultrasonic agitation in petroleum ether for 3 minutes. The pin was attached to the pin holder before it was attached to the lever of the apparatus. The direction of sliding in relation to the pin was always known because the pin and the holder were attached in the same way every time. The tests were carried out with two identical pin holders. This arrangement shortens the time between the tests. Before the pin holder was fully tightened, the perpendicularity of the lever had to be checked with a level. The disc was attached to the holder with two screws. The aluminum rings and other filling material were used, if necessary, to fix the disc in the middle of the holder. In this case aluminum foil and thin plates were used in some of the tests as extra fillings. The flatness of the disc was checked with a dial indicator and possible deviations were corrected until the deviation was 5 µm or smaller. For lubricated tests a timer was set to stop the spinning after 12 hours. The discs were lubricated with vaseline by spreading a smooth layer to the surface of the disc before the test is started. The tests were started by turning the apparatus on and adjusting the spinning speed to the value of 95 RPM. When the disc was spinning the pin was set down gently to start the test. All iron grades were tested three times in dry sliding and four grades were tested also with lubrication, two times each. Operating variables used in the wear tests are listed below.

Operating variables:

- Motion: Continuous unidirectional sliding
- Velocity: 95 rpm, 0.1 m/s
- Normal Load: 5 N
- Temperature: 22°C
- Sliding time: 42 min/ 12 h (dry/lubricated)
- Sliding distance: 250 m / 4300 m (dry/lubricated)
- Atmosphere: Laboratory air, 50 ± 10 % relative humidity
- Number of tests: 3 without lubrication/ 2 with lubrication
- Wear track: Diameter 20 mm

After the test, both the disk and the pin were cleaned the same way as prior to the test. The wear surfaces were inspected and photographed with an optical microscope and the samples were stored in a plastic box for later examination.

4.5 Sample measurements and documentation

4.5.1 Pin wear

After the test the pin was cleaned with ultrasonic agitation in petroleum ether. The pin was inspected and photographed with an optical microscope when it was still properly attached to the pin holder. The wear track in the pin was an ellipse. All the pins were photographed with the same magnification and as many picture as necessary were taken from the same pin to document the whole wear track. Pictures were attached together if necessary and the size of the wear track was determined with the help of a scale bar. An example of the wear track is shown in Figure 19. The area of ellipse wear track can be calculated by equation (4), where x and y are the two radii of the ellipse.

$$A = \Pi xy \qquad (4)$$

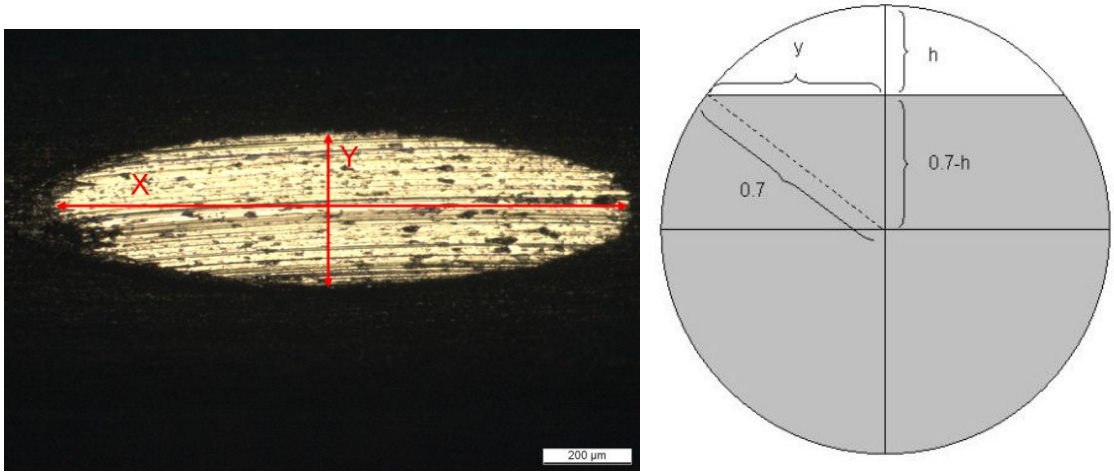

Figure 19. *The wear track of the pin from test 12 and the cross section of the worn wire.*

The worn part of the steel wire has a shape of half ellipsoid. The volume of the wear loss can be calculated by using the equation (5) where the volume of ellipsoid is divided by two. The height of the worn part (h) can be calculated with equation (6) when the diameter of the wire is known. Figure 6 illustrates the cross section of the wire at the widest point of the wear track. Equation (6) is derived from the Pythagorean and quadratic equations. The dimensions in equation (6) are given in millimetres.

$$V = \frac{2}{3}\Pi hxy, \tag{5}$$

where:

h is height of the wear track
x is half of the length of the wear track
y is half of the width of the wear track

$$h = \frac{\left(1.4 - \sqrt{\left(1.96 - 4y^2\right)}\right)}{2} \tag{6}$$

4.5.2 Disc wear

Similarly with the pins, also the discs were cleaned and photographed with an optical microscope. The width of the wear track can be estimated from the microscopic pictures. The width was used as the guiding dimension when evaluating the profile data. An example of a wear track in the disc can be seen in Figure 20. The profile of the worn surface of the disc was measured with a profilometer in VTT, Otaniemi. Three measurements were taken for each disc from appropriate random places. An appropriate place means that there were no visual flaws or scratches in the measurement path. Each measurement was taken across the wear track with the distance of 2 mm. Profile data consists of 4000 x and y coordinate points. This means that the y- coordinate is measured at every 5 μm.

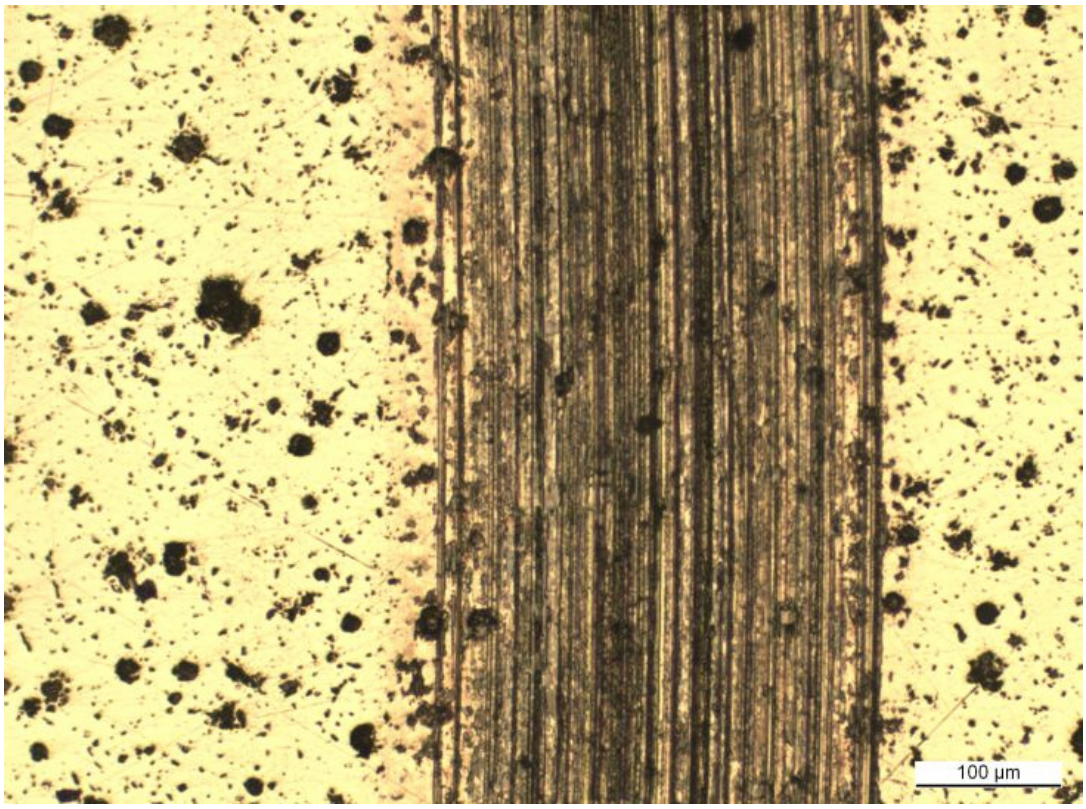

Figure 20. *An optical microscope picture of a wear track in GJS-600-10 disc, test 30.*

The volume loss for the disc can be calculated from the profile data. The first thing was to solve the worn area from every measurement by creating graphs from the profile data. An approximation of the initial surface was added to the graphs and the worn area was compared to this curve. Then the width of the wear track was used as a guide to locate the exact place of the groove. It was noticed that the disc wear was not always positive. In some cases there were peaks in the wear data curve that reached above the initial surface line. This means that at these points wear gets negative values, i.e., material transfer from the pin to the disc has occurred. This material could be transmitted from the pin due to adhesion. Graph 2 illustrates the measured profile, the initial surface line and the location of the wear track. The worn cross-sectional area was calculated by mathematical methods and the average of the three tests was determined. The volume loss can be calculated when the worn cross-sectional area, wear track diameter and wear track width are known by using equation (7).

$$V = \Pi a(d - w), \tag{7}$$

where:

a is the worn cross-sectional area
d is the diameter of the wear track
w is the width of the wear track

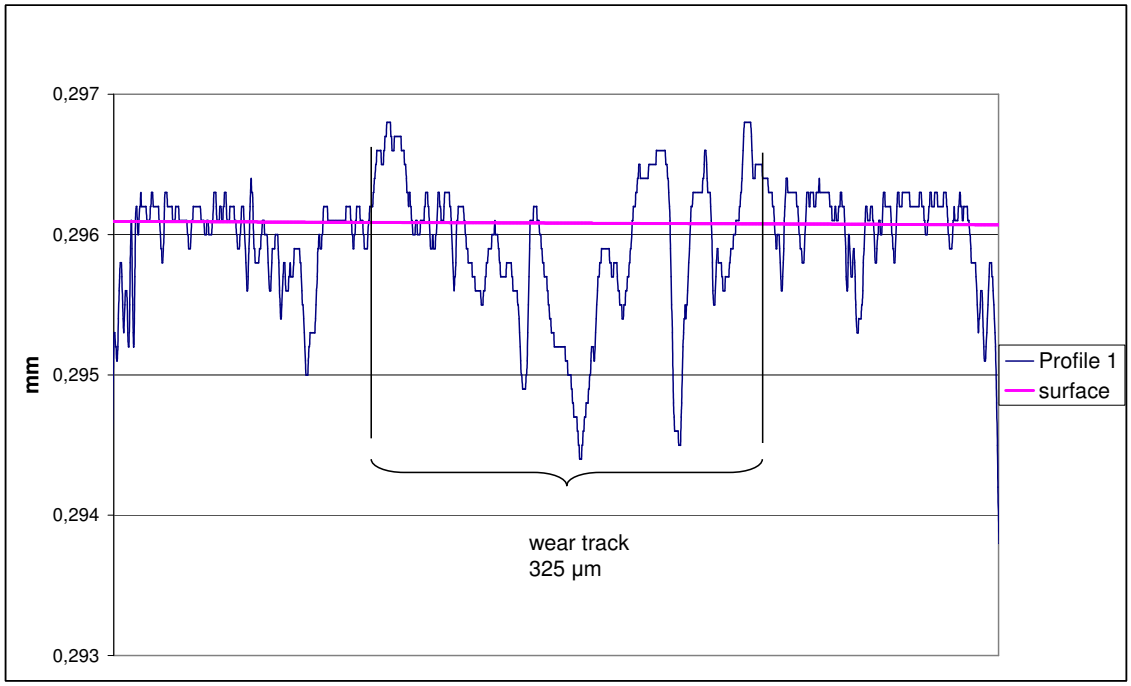

Graph 2. *An example of profile data curve and the method for determining the worn cross-sectional area.*

4.5.3 Friction

During the wear tests, the friction force that acts through the pin was measured. In dry sliding test the friction force was measured every 500 ms and in lubricated tests every 10 s. For the graphs, friction force was converted to the coefficient of friction (COF) and time was converted to the sliding distance. Friction force can be converted to COF by dividing the friction force (F_f) by the normal force (F_n) as shown in equation (8) [18]. The normal force in the actual tests was 5 N. For each test the average coefficient of friction was calculated. An example of the friction coefficient vs. sliding distance curve is presented in Graph 3. These graphs were used to compare the friction behavior of the different ductile iron grades and also to see how the lubrication influences the coefficient of friction.

$$COF = \frac{F_f}{F_n} \tag{8}$$

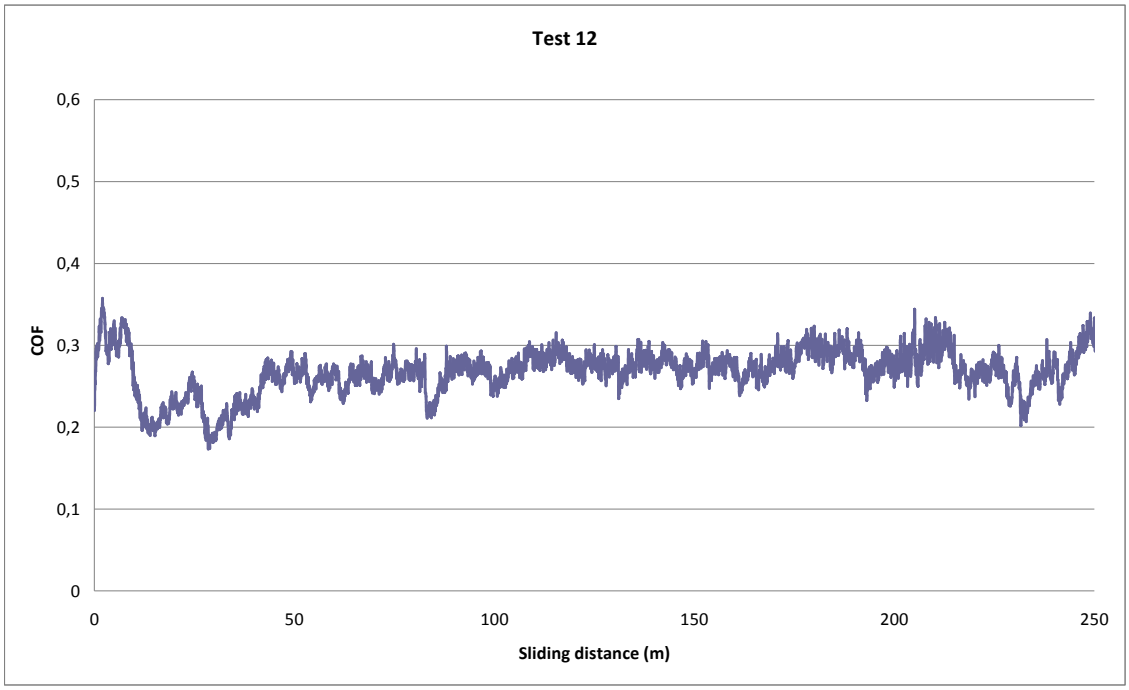

Graph 3. *The coefficient of friction as a function of sliding distance, test 12.*

5 RESULTS

5.1 Pin wear

5.1.1 Dry sliding

Total number of 31 dry sliding tests were carried out in this thesis work. All ductile iron grades were tested three times except the GJS-1200-3 which was tested four times. The volume loss for the steel wires was calculated by using the equations and methods mentioned in the previous chapter. There was large variation in the size of the wear track and this can be seen in Appendix 3 where all dry sliding test results are presented. Averages have been calculated from the three test results carried out for every grade. Grades GJS-500-7, GJS-400-15 and GJS-500-14 are exceptions because in these tests there was one result which differed too much from the remaining two results. Therefore the tests 2, 7 and 29 were left out from the average calculations. Figure 21 is an example of the size difference between two wear tracks measured from the tested steel wires. The large wear track is from test 5 and the small wear track is from the pin used in test 7. The material used in these two tests was GJS-500-7. Both images are in the same scale.

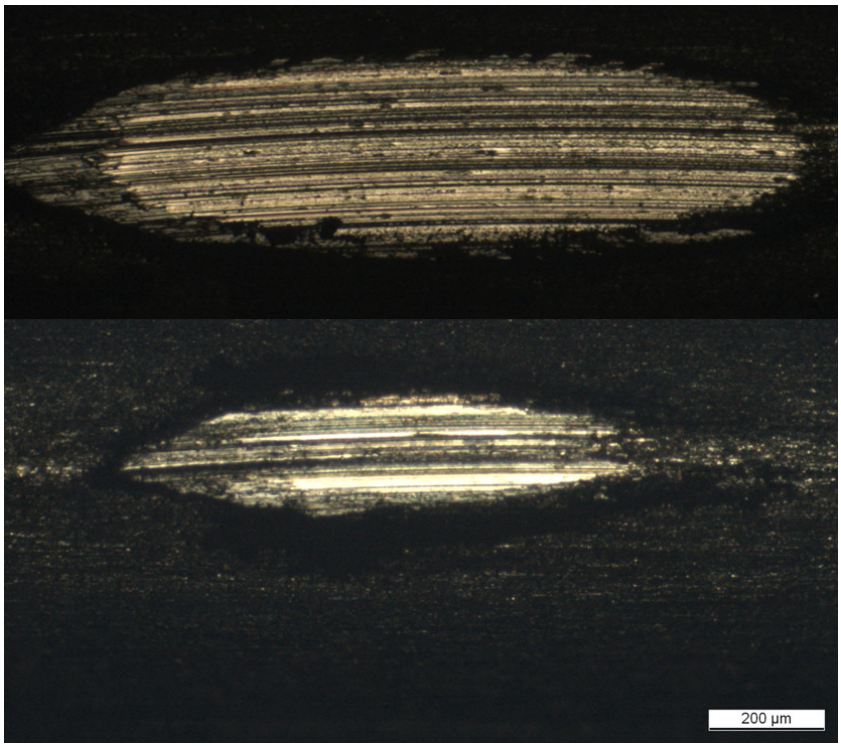

Figure 21. *Pin wear tracks from tests 5 and 7. Sliding direction is from left to right.*

In most cases there was visible wear debris on the rear end of the pin after the tests. It was loose enough to be shaken off and the rest of it was cleaned with ultrasonic agitation. A couple of pins were photographed both before and after the ultrasonic cleaning. Figure 22 shows that there is some wear residue left in the image taken from the front end of the wear track before cleaning. For reference, Figure 23 presents the same wear track after cleaning. Both images are taken from the same pin, at the same end and with the same magnification. These images are from test 9, where the disc material was GJS-600-3. There were visible unidirectional wear scars on the surface of all pins used in dry sliding tests. In some of the pins there were many small scars and the others had only a few, but big wear scars.

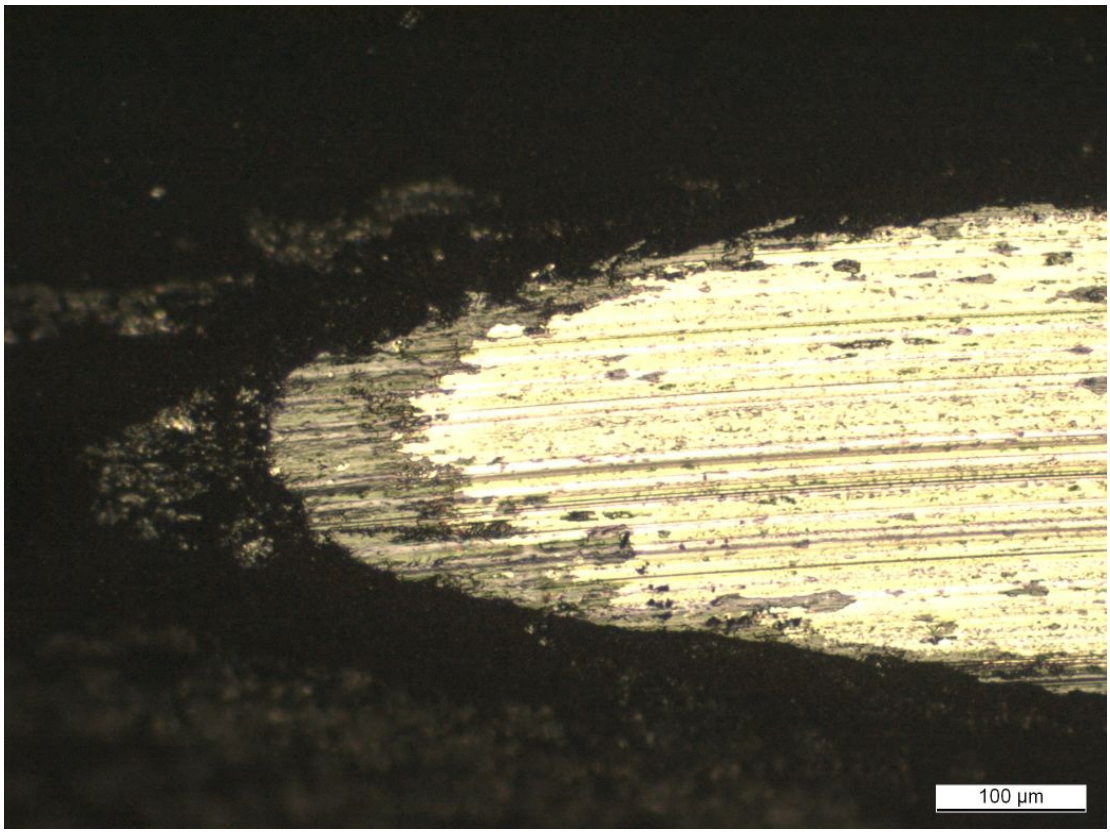

Figure 22. *The front end of the wear track from test 9 before cleaning.*

The average pin wear losses calculated in Appendix 3 are combined and presented in Graph 4. The graph shows the wear rate (10^{-6} mm^3/Nm) of the pin obtained with all tested ductile iron grades used in the disc. A trend can be clearly seen from the graph. The pin wear slightly increases along with the increasing tensile strength of the disc material. Austempered grades seem to make an exception. The largest pin wear occurs with all three austempered ductile iron grades. Pin wear is equal for the GJS-600-3 and GJS-600-10 grades. The pin seems to wear only one half of the amount against GJS-600-10 as compared to the wear against GJS-700-2.

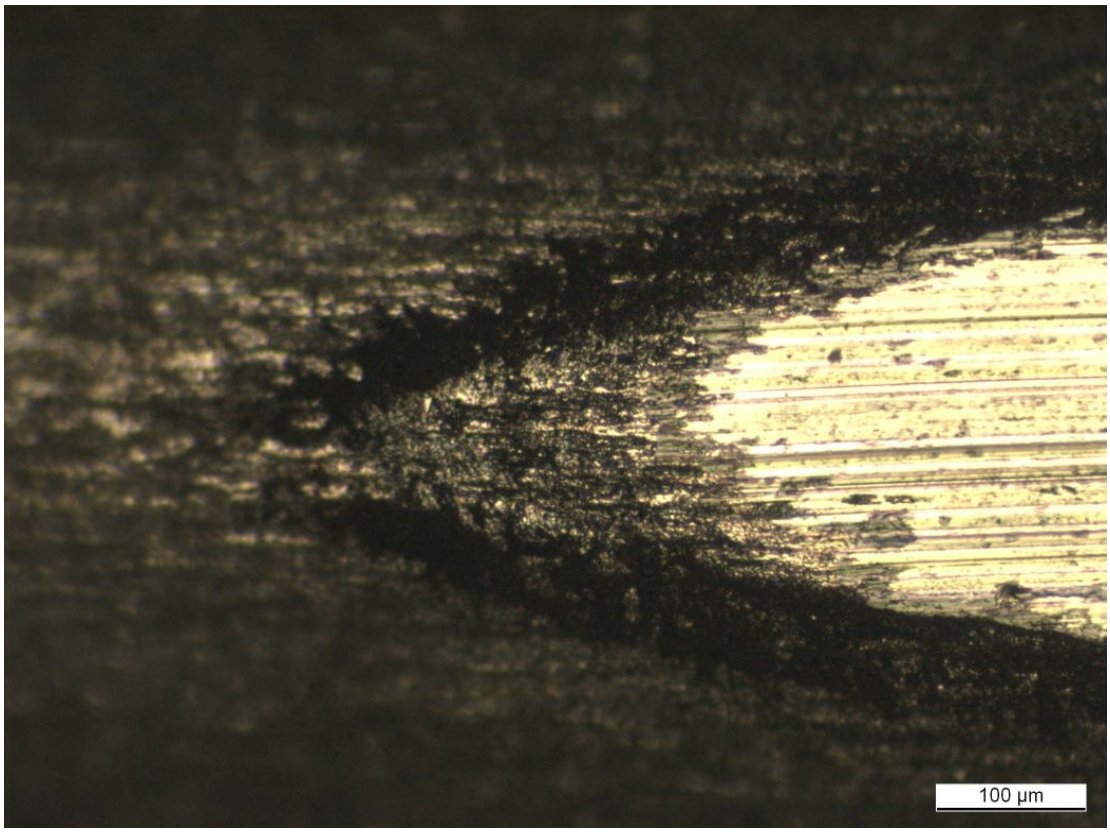

Figure 23. *The front end of the wear track from test 9 after cleaning.*

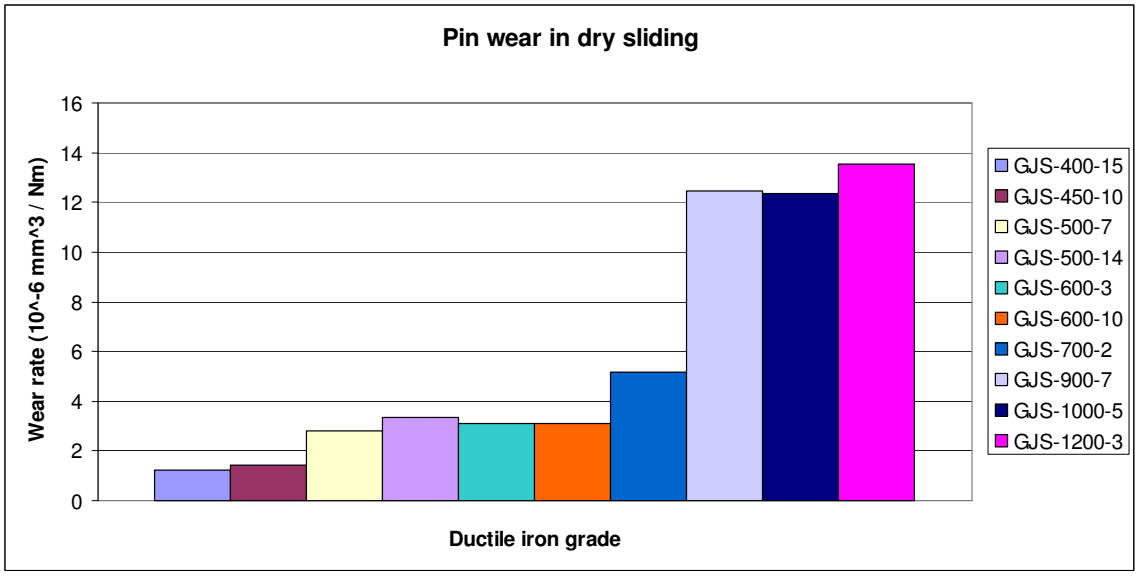

Graph 4. *Pin wear in dry sliding tests for different ductile iron grades.*

5.1.2 Lubricated sliding

In addition to dry sliding tests, four ductile iron grades were tested with lubrication and extended sliding distance. Materials for lubricated sliding tests were selected so that there was a selection of different microstructures and physical properties. All four grades were tested two times. The results of the lubricated sliding tests are presented in

Appendix 4. According to the results and friction curves, grades GJS-450-10 and GJS-600-10 showed repeatable behaviour under lubrication. The other two studied grades, GJS-700-2 and GJS-1000-5, seemed to be totally different when the lubricated and unlubricated test results obtained with the same disc material were compared with each other. Possible reasons for this are studied in more detail with the friction curves later on. The results from the lubricated tests with these two materials have so large scatter that no definite conclusion can be drawn on them.

The pin wear in lubricated tests is compared to the pin wear measured in dry sliding tests with the same materials in Graph 5. Because the wear is given as wear rate, the dry and lubricated tests are comparable despite of the different sliding distances. The sliding distance in the tests with lubrication was about 17 times longer than that in dry sliding tests. The pin has worn slightly less in lubricated condition with GJS-600-10 than with GJS-450-10. Noticeable in the GJS-600-10 material is its high elongation. According to the standards both grades should have at least ten percent of elongation. The GJS-600-10 grade used in the tests had the elongation value of more than 20 percent. This is due to the solution strengthening of this ductile iron with silicon. Silicon percentage in GJS-600-10 discs used in the lubricated sliding tests was 4.14 %. The pin wear results in dry sliding tests showed that the pin was worn more than twice as much with GJS-600-10 when compared to the pin wear with GJS-450-10. The results indicate that lubrication has a significant effect on the wear rate of the pin, especially with the GJS-600-10 grade.

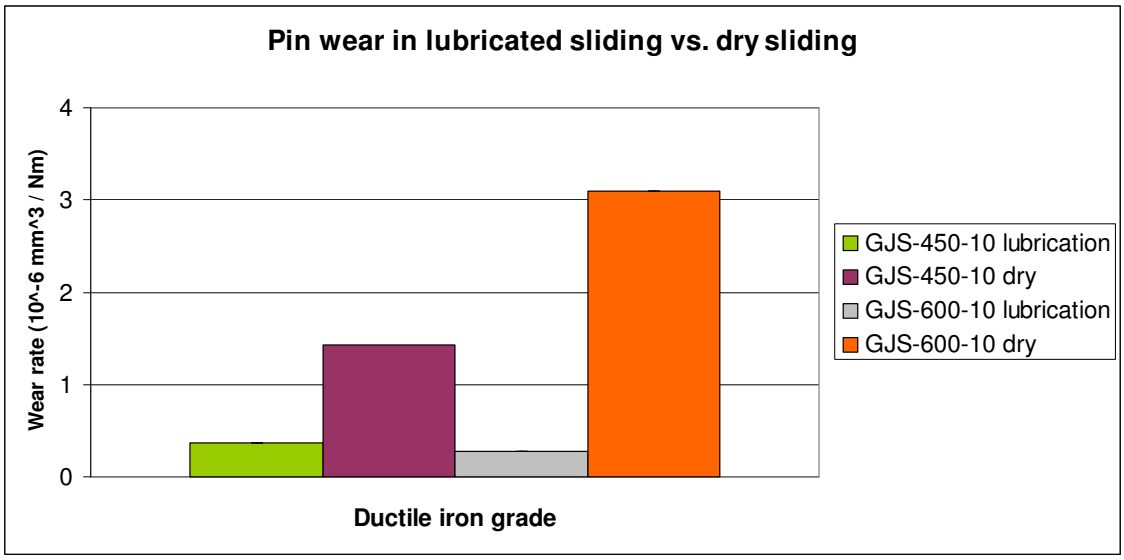

Graph 5. *The pin wear rate under lubricated and dry sliding conditions for the GJS-450-10 and GJS-600-10 grades.*

The images of the wear tracks obtained in the lubricated tests show that the surface of the track is smoother than the ones obtained in the dry sliding tests. In most of the lubricated pins, there seem to be a few larger scars visible in the wear track. The scars might be due to the three body abrasion. The front edge of the wear track also looks

different in lubricated tests. An example of the image taken from the pin used in lubricated test is presented in Figure 24.

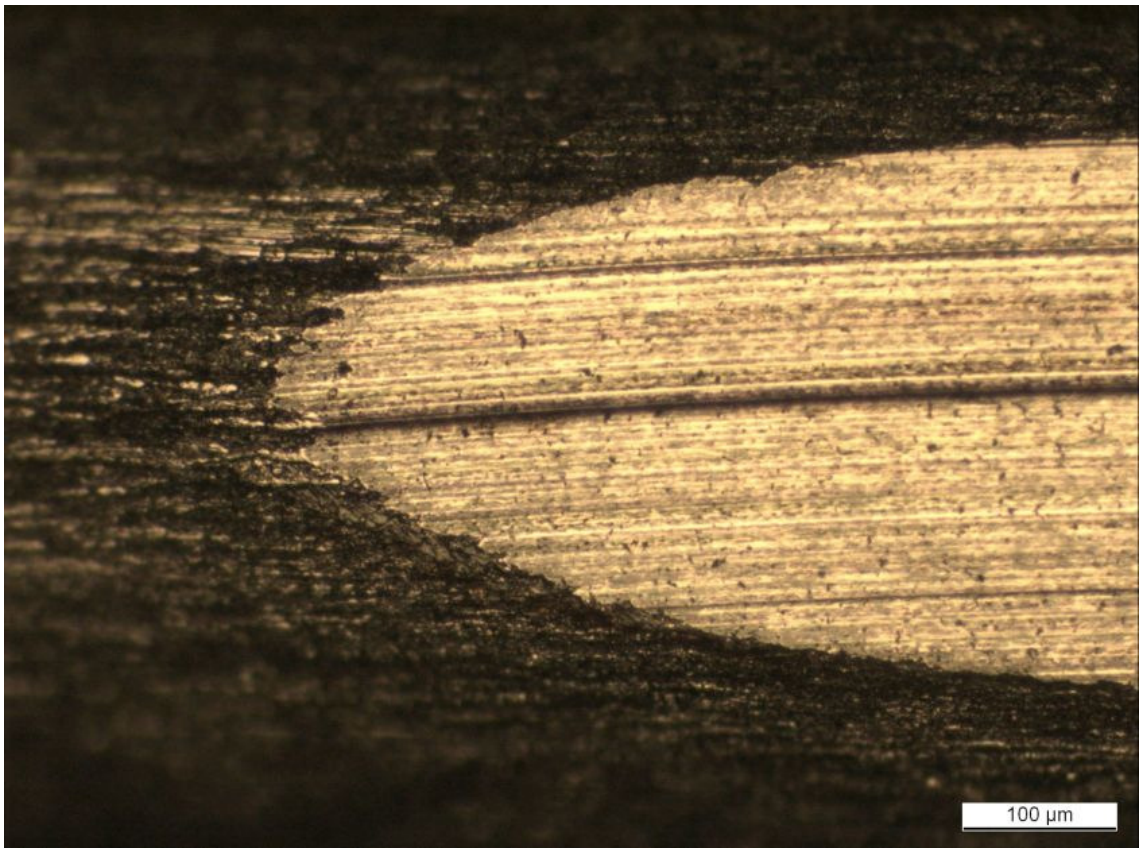

Figure 24. *The front end of the wear track obtained in the lubricated test 39, GJS-600-10.*

5.2 Disc wear

5.2.1 Dry sliding

Microscopic studies of the worn discs revealed a great variety in the width of the wear tracks. The width of the wear track is only used for making the analysis of the profile data easier. The wear track profile data turned out to be quite difficult to analyze. This is due to the fact that the wear tracks do not manifest themselves so clearly. In other words, the wear tracks were not as deep as expected. This is where the width of the track comes useful. It helps to locate the area of the track in the measured surface profile curve. The microscopic images also reveal more than just the width of the track. There are signs of material transfer, dry lubrication by graphite and major wear scars in the discs. The figures 25 and 26 are taken from tests 15 and 24. The materials used in these tests were GJS-600-3 and GJS-1000-5. The image from test 15 is a good example of a disc that has worn a lot. The disc from the test 24 is an example of a disc which has received material from the pin and the resulting cumulative volume loss is negative.

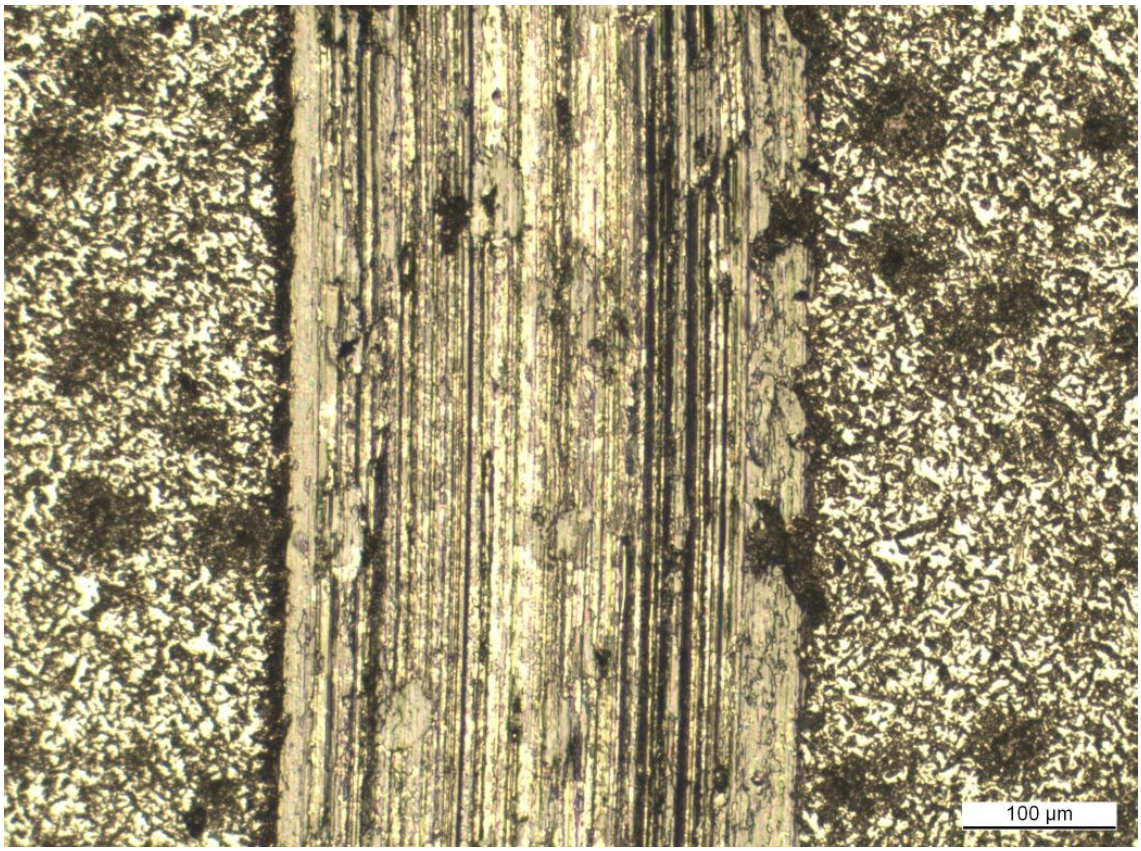

Figure 25. *A wear track image from the disc used in the test 15 where the disc material was GJS-600-3.*

The microscopic images suggest that graphite inclusions are at least partly worn off and that they are spreading around the wear track acting as dry lubricant. The graphite inclusions can be seen in the profile curves as large holes and it is important not to take them into account when determining the wear track edge points from the measured surface profile curve. The profile data from the discs has a definite amount of scatter which is compensated by excluding some single profile measurements. The scatter is probably a result from the quite small amount of wear in relation to the surface roughness. In spite of these minor challenges the wear for each ductile iron grade could be determined and the results are presented in Graph 6.

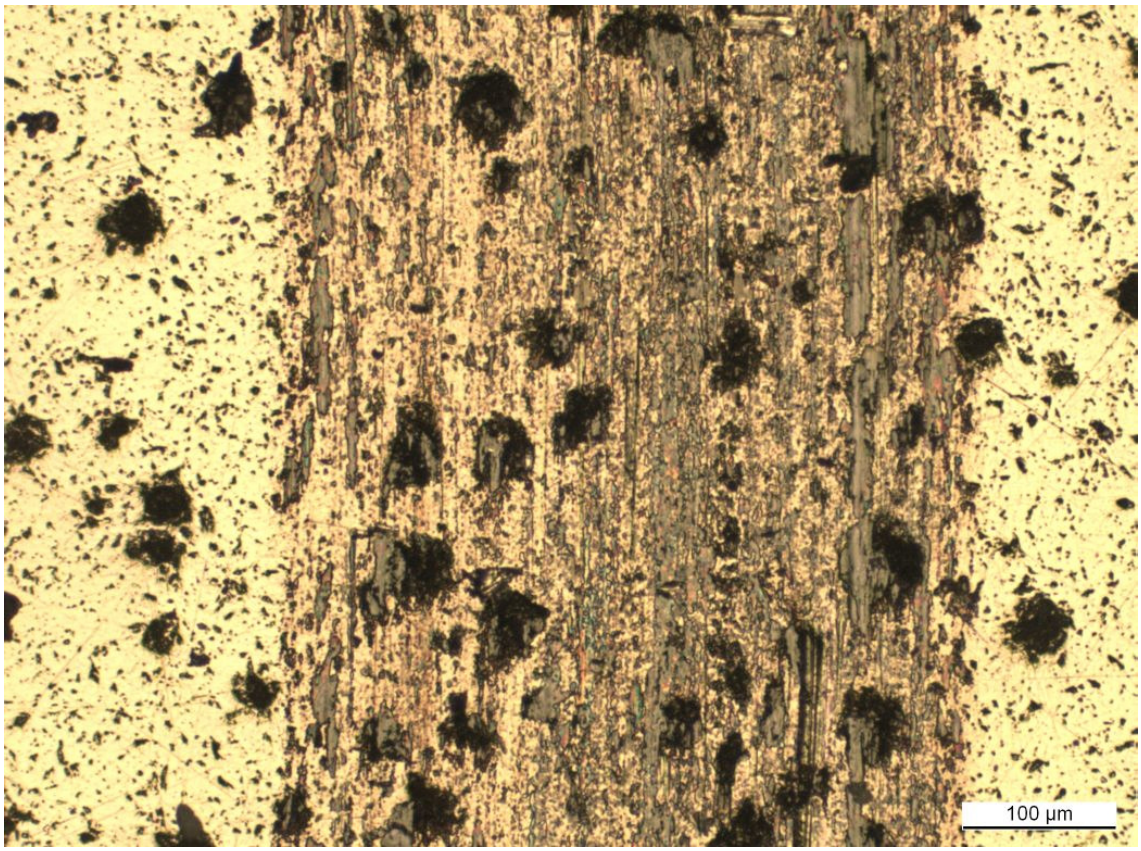

Figure 26. *A wear track image from the disc used in the test 24 where the disc material was GJS-1000-5.*

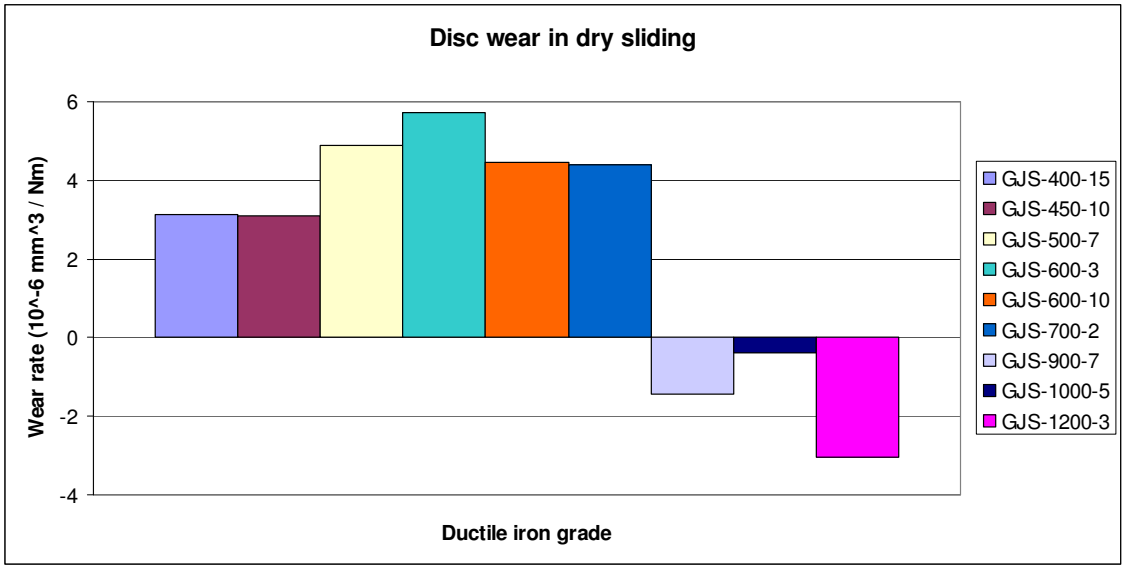

Graph 6. *Disc wear in dry sliding measured with different ductile iron grades.*

The results in graph 6 show that the wear of the austempered grades is negative, meaning that there is more material adhered from the pin to the discs than what is worn off. Another observation is the low wear rate of the softest ferritic grades GJS-400-15 and GJS-450-10. There can be a number of reasons why these two grades seem to wear less than expected, but this question is addressed in the following chapter. In addition,

one noticeable fact in the disc wear results is the lower wear rate of the solution strengthened ferritic grade GJS-600-10 as compared to the corresponding grade GJS-600-3. The wear rate of GJS-600-10 is equal to that of GJS-700-2.

5.2.2 Lubricated sliding

As already mentioned in the previous chapter, all wear tests with lubrication were not successful. The scatter of the wear results on GJS-700-2 and GJS-1000-5 was very large and as only two tests were carried out for both of these materials, no reliable conclusions can be drawn from these results. The repeatable results from the tests made with GJS-450-10 and GJS-600-10 showed that the GJS-600-10 grade is more wear resistant material under lubricated sliding than the grade GJS-450-10. Graph 7 shows that the wear rate of GJS-450-10 is more than twice the wear rate of GJS-600-10 in lubricated sliding. It is interesting to note that there is a great difference in the wear rate between the dry and lubricated tests of GJS-600-10, whereas the grade GJS-450-10 shows smaller difference. It was also noted that the profile measurement results of the lubricated tests had less scatter than the corresponding results from the dry tests.

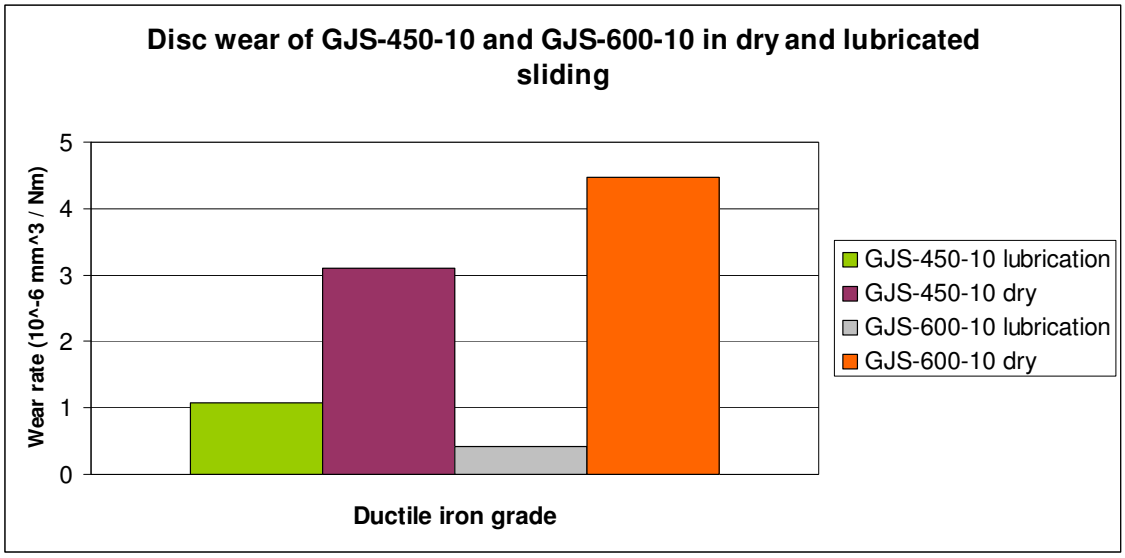

Graph 7. *Wear rates in cubic millimeters / Nm for GJS-450-10 and GJS-600-10 as measured with and without lubrication.*

A microscopic wear track image from the lubricated wear test 37, where the disc material was GJS-600-10 (solution strengthened ductile iron), is presented in Figure 27. Light in this image comes from the side so that the topography of the surface could be seen more clearly. On the left hand side of the image it can be seen how the graphite inclusions increase the roughness of the disc surface. The image also shows that the disc has only a small amount of wear. The surface seems to be flattened in the wear track area and there are only a few visible grooves. In this sense the surface of the wear track in discs is similar to the tracks in the pins.

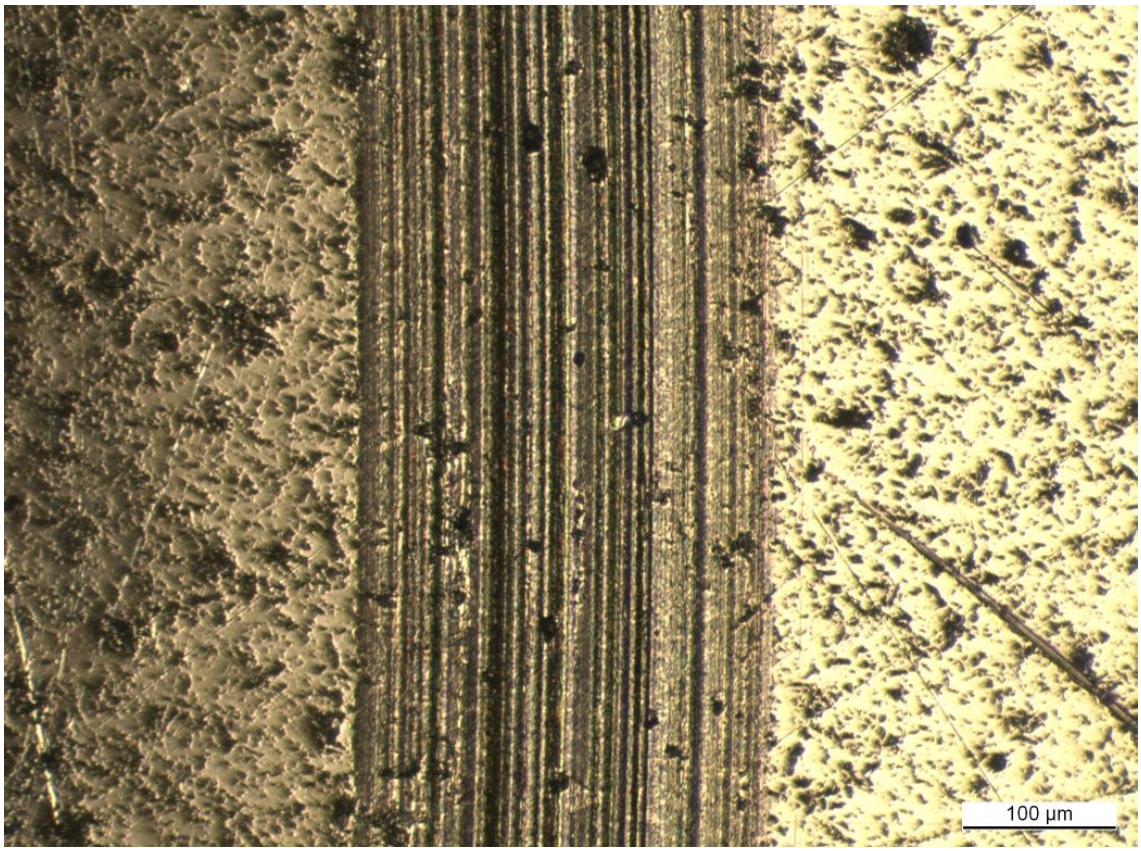

Figure 27. *A wear track image from the disc used in the test 37 where the disc material was GJS-600-10.*

5.3 Friction behaviour

5.3.1 Dry sliding

All the measured friction data of the wear tests were plotted as curves in the graphs to make the comparison between the different tests easier. The average coefficient of friction was calculated for each test and the averages with the standard error bar for each iron grade are presented in Graph 8. The coefficient of friction seems to increase along with increasing tensile strength and again the ADI- grades stand out with a larger COF in relation to the trend. Graph 9 illustrates that there is also a positive correlation between the pin wear and COF. The COF seems to increase along with the hardness of the disc.

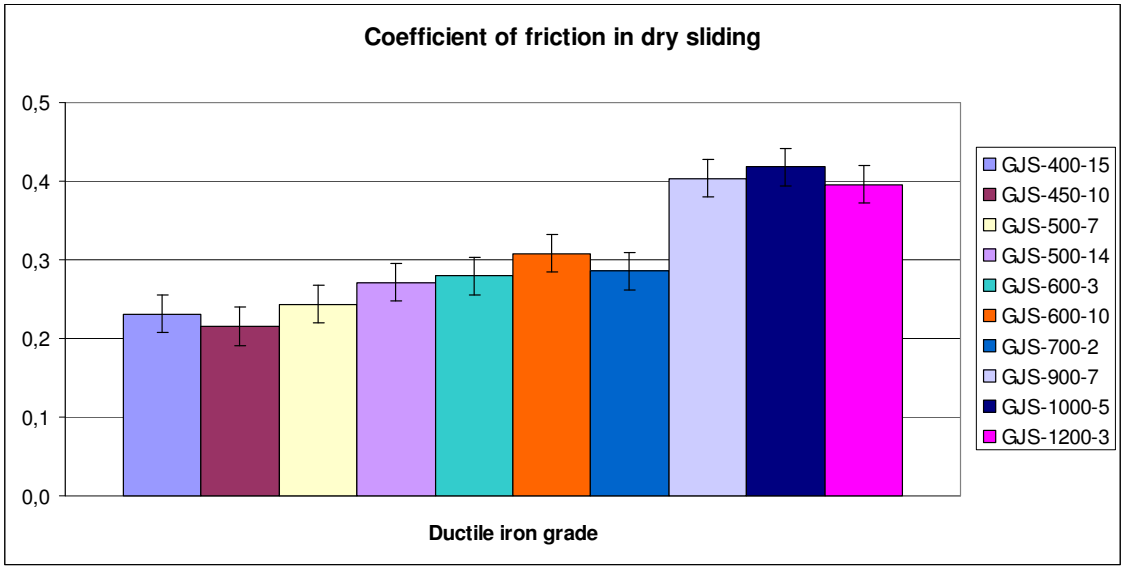

Graph 8. *The average coefficient of friction in dry sliding with steel against different ductile iron grades.*

The friction versus sliding distance curves give good information whether the test is successful or not, when they are compared against the other tests with the same disc material. For instance, all the discarded tests 2, 7 and 29 have friction curves different from the other tests. A similar feature of all discarded test results is a smaller COF. It is hard to tell why these tests show smaller COF and different friction behaviour but it can be seen that this has influenced also the wear results. Test 2 shows an interesting pin wear result as compared to the other discarded tests. The pin wear is greater in test 2 than in the other two tests made with GJS-400-15. As expected, the pins are less worn in tests 7 and 29 where the COF is lower.

The friction curves have a similar trend with all iron grades. There is a peak in the beginning of the friction curve, where the COF first rises rapidly and then comes down. After the peak the COF usually increases slowly till the end of the test or stays at a constant level reached right after the peak. The differences in the curves among the ductile iron grades are normally in the height and sharpness of the peak and in the slope of the curve after the peak. For example, GJS-900-7 has a really sharp and high peak where COF goes up to 0.6 in the beginning and then the curve normalizes after sliding about 20 metres. Instead, the friction curves with GJS-700-2 show hardly any peak and the increase of COF is minimal during the tests. Graph 10 presents an example of typical friction curves for both GJS-700-2 and GJS-900-7. The curves are plotted as a moving average over the sliding distance of 5 metres to make the curves smoother and the trends easier to recognize.

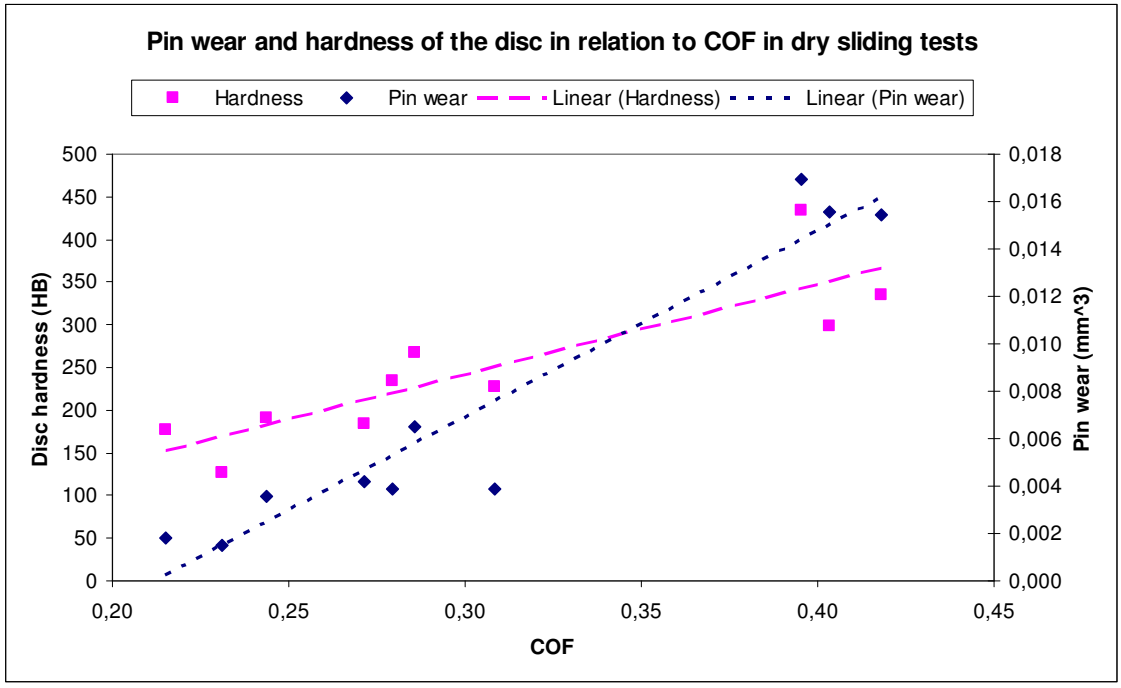

Graph 9. *Pin wear in relation to COF and COF in relation to disc hardness in dry sliding tests.*

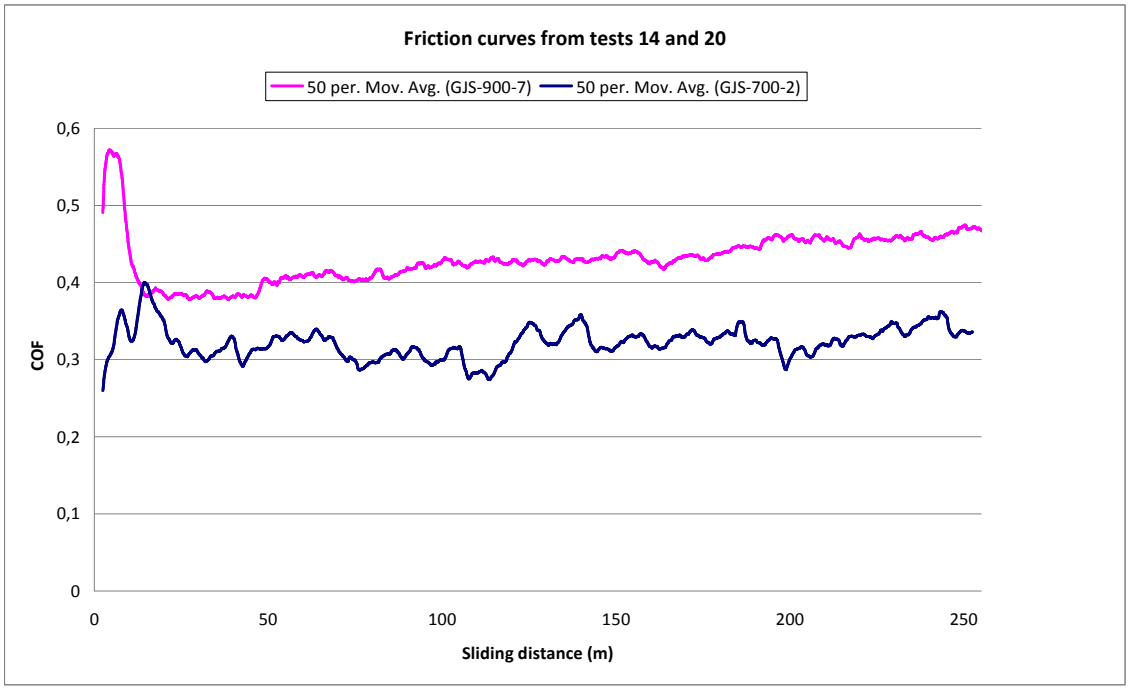

Graph 10. *Typical friction curves of GJS-700-2 and GJS-900-7 presented as the moving average over the sliding distance of 5 meters.*

5.3.2 Lubricated sliding

According to the test results of lubricated sliding, COF seems to be higher with lubrication, when GJS-450-10 is used as a disc material. This might be due to the sliding distance, which is many times longer in lubricated tests and due to the fact that during the

tests the lubricating effect fades off. On the other hand, GJS-600-10 shows almost the same COF in both cases. Graph 11 presents the COF averages for GJS-600-10 and GJS-450 under both test conditions. Typical friction curves under both test conditions and for both materials are presented in Graph 12. The curves are plotted as a moving average of 50 measurement points. The upper x-axis is for dry sliding friction curves and lower x-axis for lubricated condition.

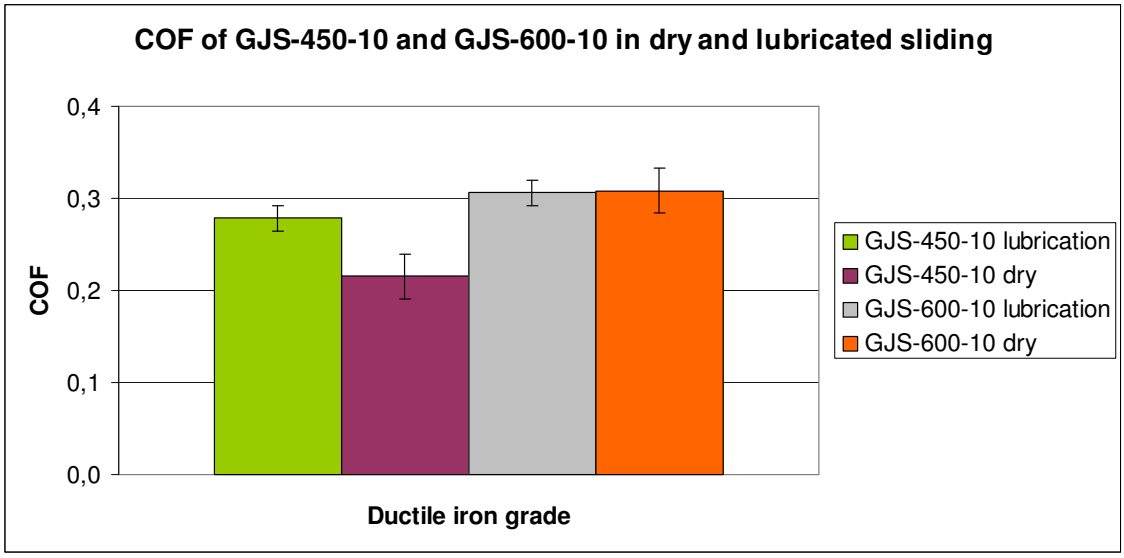

Graph 11. *COF of GJS-450-10 and GJS-600-10 against steel in dry and lubricated sliding.*

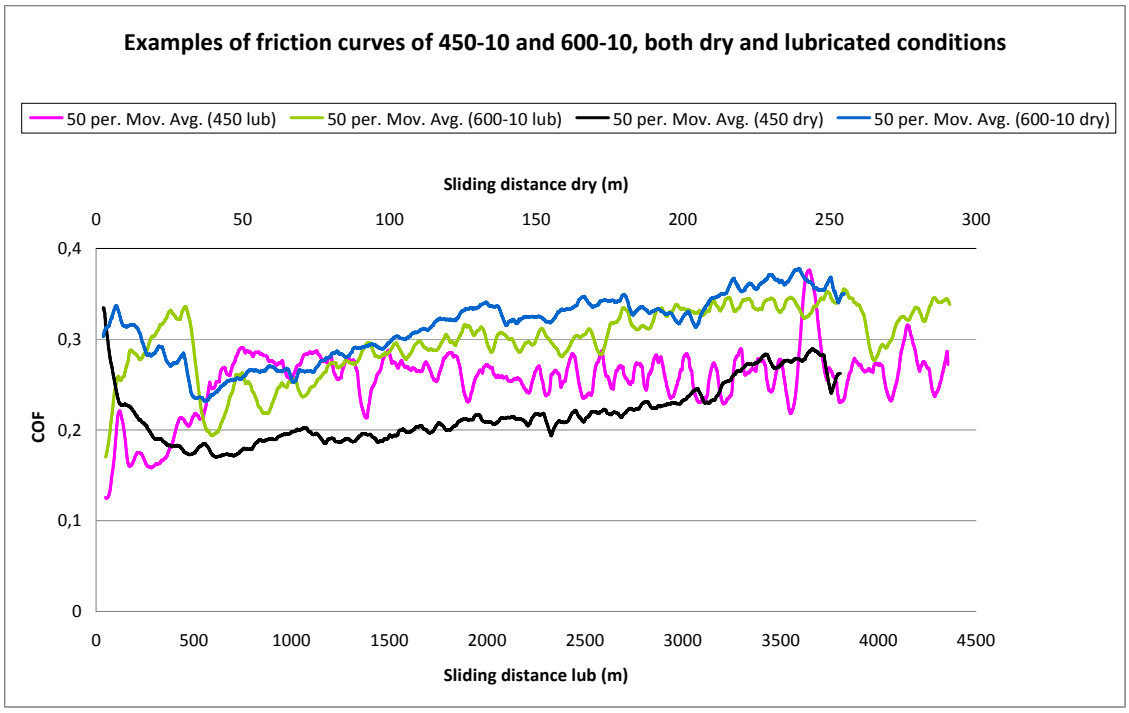

Graph 12. *Typical friction curves obtained in dry and lubricated tests with GJS-450-10 and GJS-600-10.*

As mentioned previously the friction curves give useful information on the events during the test and not only on the final result as the pin and disc wear tracks do. The both friction curves of the repetitive tests on GJS-450-10 and GJS-600-10 measured with lubrication are similar to each other whereas the lubricated friction curves obtained with GJS-700-2 and GJS-1000-5 differ a lot from each other. Graph 13 presents the lubricated friction curves of tests 18 and 26, where the disc material is GJS-700-2. The curve from test 26 shows that the lubricating effect fails after 1000 metres and COF starts to increase. The friction behaviour in test 18 looks quite reasonable as there is a little bit higher COF in the beginning before the surface roughness has worn off. The COF in the test 18 reaches a constant level after sliding of about 1000 metres. This constant level equals to the COF in the test 26 before lubrication failure.

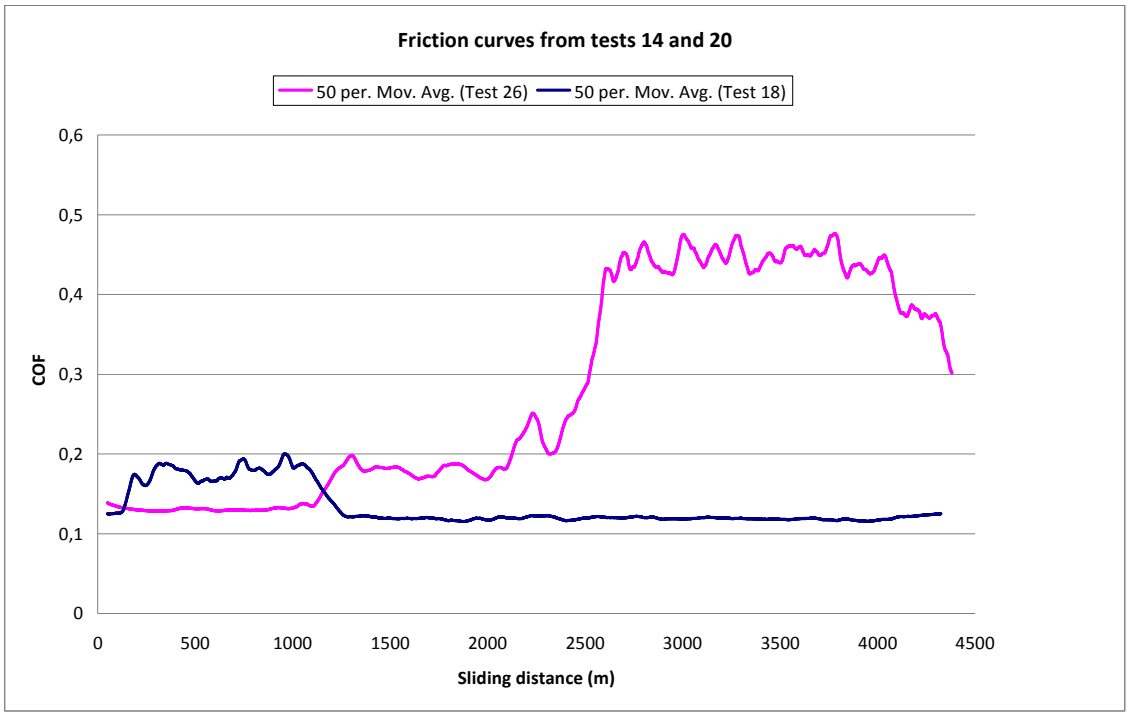

Graph 13. *The friction curves of GJS-700-2 obtained in repetitive lubricated sliding wear tests. The curves are plotted as a moving average over the sliding distance of 50 metres.*

6 DISCUSSION OF THE RESULTS

6.1 Overview of the tests

As a summary the experimental part of the thesis was successful in spite of the fact that some of the wear tests had to be excluded due to the largely different results. The designed sample holder was working as planned and it can be stated that all the effort and time spent in the design process was worth of it. The test parameters, which were selected on the basis of the preliminary test results, seemed to be a good compromise for all the test materials, although the wear could have been a bit more severe. The sample preparation went out without any major problems. Mechanical properties and chemical compositions of the test materials were a great benefit which came along because the discs were machined from the tensile test bars. The size of the discs, in the other hand, was a small disadvantage because it limited the possibilities of gaining sliding distance.

6.2 Pin wear

The evaluation of the pin wear was quite straight forward as the size of the wear lens was easy to measure from the microscopic images. Great differences were observed already visually in the pin wear between different ductile iron grades. The pin was worn a lot against ADI grades. It is possible that the surface of the disc work hardens during the test, which increases the surface hardness of ADI leading to the more severe pin wear. The surface hardness was not measured after the tests to proof the existence of work hardening. Of course, all ADI grades are already initially harder than the other ductile iron grades used in this study. The wear rate of the pin looks to be in relation to the tensile strength of the disc and it increases along with the strength of cast iron disc. GJS-600-10 shows promising pin wear results when compared to the grades GJS-600-3 and GJS-700-2. The solution strengthened ferritic ductile iron GJS-600-10 is similar to GJS-600-3 and shows better pin wear results than GJS-700-2. It is hard to explain why lubrication has a stronger influence in the case of GJS-600-10 than GJS-450-10 in both pin and disc wear. Maybe the GJS-600-10 is able to absorb more lubricant than GJS-450-10 does. The differences in nodule counts may influence lubricant absorption. Unfortunately, information on the nodule count of the GJS-600-10 was not available for comparison.

6.3 Disc wear

The disc wear evaluation consisted of the microscopic study of the wear track, of the surface profile measurements and analysis of the profile data. Even if every disc was treated and measured in the same way there are still many factors which created scatter to the results. Standard deviations for every iron grade under both dry and lubricated conditions are presented in Table 9. It must be mentioned that in some cases the standard deviation is calculated only from two test results. Suggestions for further studies are discussed in the following chapter. The geometry of the pin and continuously changing contact area make it difficult to calculate and estimate the wear rate of the tested materials with wear equations and wear maps.

Table 9. *Standard deviations of tested ductile iron discs under both dry and lubricated conditions.*

DRY					
Material	**Wear rate 10^{-6} mm^3/Nm**			**Standard deviation**	**Notice**
GJS-400-15		3,041	3,234	0,136	Only 2 tests
GJS-450-10	7,680	0,015	1,608	4,044	
GJS-500-7		4,020	5,765	1,234	Only 2 tests
GJS-500-14	-0,118	0,935	14,373	8,080	
GJS-600-3	8,627	5,299	3,279	2,701	
GJS-600-10	8,551	1,837	3,003	3,587	
GJS-700-2	4,435	3,379	5,393	1,007	
GJS-900-7	3,170	-2,508	-4,951	4,166	
GJS-1000-5	-4,446	4,317	-1,007	4,415	
GJS-1200-3	-0,934	-1,630	-6,568	3,072	
LUBRICATION					
Material	**Wear rate 10^{-6} mm^3/Nm**			**Standard deviation**	**Notice**
GJS-450-10	1,205	0,954		0,178	Only 2 tests
GJS-600-10	0,287	0,562		0,194	Only 2 tests
GJS-700-2	0,054	1,003		0,671	Only 2 tests
GJS-1000-5	0,340	3,430		2,185	Only 2 tests

Again the ADI grades showed different results as compared to the other ductile iron grades. This time the disc wear behaviour in cases where ADI was involved was outstanding. ADI grades appeared to wear much less than the others. Actually, the wear rate was negative meaning that there was more material transferred from the pin to the disc than was worn away. These results agree well with the previous studies presented in the theoretical part, where it was shown that ADI is three or four times more wear resistant than pearlitic ductile iron in this type of sliding motion. The further studies with SEM would give more information on the actual wear mechanisms. The literature, referred in the theoretical parts, suggest that delamination is the predominant wear mechanism in most of the cases.

The reason why the two ferritic ductile iron grades GJS-400-15 and GJS-450-10 are less worn than the ferritic/pearlitic and pearlitic grades might be ploughing. This means

that material is moved to the sides of the groove without the removal of material. The ridges formed this way lower the worn area in the profile measurements. Ferritic ductile iron grades could act this way as they are softer and more ductile than the other iron grades used in the tests.

The disc wear results show that the solution strengthened ferritic ductile iron GJS-600-10 is more wear resistant than GJS-600-3 and comparable to GJS-700-2. Unfortunately the second high silicon grade GJS-500-14 had a lot of difference between the repetitive test results and had to be discarded from the results. It is hard to conclude the influence of silicon alloying on the wear resistance based on only one test material. As already mentioned, Lerner's [31] test results indicate that silicon alloying has a positive influence on the wear resistance of ductile iron. It was not explained how the silicon alloying makes ductile iron more wear resistant, even though it slightly reduces the hardness. The graphite inclusions may work as dry lubricant more efficiently in silicon alloyed ductile irons than without silicon alloying. Another explanation can be more ductile and deformable matrix of the solution strengthened ferritic ductile iron grades that mean less wear debris.

6.4 Friction behaviour

The coefficient of friction seems to be increasing along with the tensile strength of the disc material. Once again the ADI grades show different behaviour as compared to the others. GJS-600-10 has a little bit higher COF than GJS-600-3 and GJS-700-2. This is considered as a positive result from the HICON viewpoint, where high friction and low wear are the goal. In addition, GJS-600-10 has shown promising results for both pin and disc wear. An interesting thing to notice was that while lubrication dramatically decreased the wear of the pin and the disc, the COF remained approximately on the same level for ductile iron grades GJS-450-10 and GJS-600-10.

6.5 Suggestions for further studies

The profile measurements of the wear tracks on the surface of the discs showed less wear than expected. There were difficulties to reveal the location of the wear track in some of the tests. In addition, the graphite inclusions on the surface and inside the worn groove made the analyzing process even more challenging. Therefore there might be a need to increase the sliding distance or the contact pressure to obtain deeper wear tracks in the disc. Sliding distance could be increased by increasing the track diameter, which means bigger discs, by increasing the spinning speed of the disc or by making the test last longer.

The surface profile was measured from three random points of the disc. Some of these profile measurements showed lots of scatter, even so that there were both positive and negative wear rate values measured from the same disc. The reason behind this might be that the disc was not perfectly parallel to the horizontal plane, even though it

was adjusted with a dial indicator. Another reason to explain this kind of scatter might be that the bottom of the groove is not equally worn around the wear track. It is possible that there are some pits and layers which can distort the measurements. To eliminate this kind of scatter, the number of surface profile measurements should be increased.

The contact pressure is problematic due to the geometry of the pin. As the pin is worn, the contact area increases and the contact pressure drops down. By increasing the normal load, there might be a risk for surface deformation in the initial stage of the test. There is also a great variety of test materials with largely different hardness values. This means that the surface of the softest and the hardest material can bear different amounts of pressure at the same normal load. Consequently it is a challenging task to select a constant set of test parameters that would work well for all materials, by creating enough but not too much wear. The diversity in the hardness of the disc material influences also the pin wear. As the test results show, pin wear generally increases along with increasing disc hardness. In the tests of this thesis the pin wear was not too dramatic, which means that the size of the pin allows the test parameters to increase towards more severe wear.

The small number of tests for each ductile iron grade was recognized already before the experiments. This was due to the tight time schedule and large number of test materials. Of course, it would be reasonable to carry out more tests for each material to increase the statistical significance of the results. Especially more lubricated tests should be carried out due to the large scatter in these tests.

Microhardness tests for the wear track of the disc could be carried out at least for ADI grades to find out whether there has been any work hardening of the surface. It was already mentioned earlier that the SEM analysis of the wear track has been left out of the thesis and that it is carried out as separate study. SEM analysis could give information on the acting wear mechanisms and also on the elements found on the surface of the wear track. It could be useful to analyze also the bottom of the wear track to see whether it is equally worn all around or whether there is some visible deformation.

7 CONCLUSIONS

The pin-on-disc wear tests against steel for different ductile iron grades have shown that there is a significant difference in the wear behaviour between austempered grades and all the others. ADI grades are wear resistant but at the same time the pin wear is the highest in sliding wear against austempered ductile iron grades. In addition, ADI grades assume the highest coefficient of friction. Lubricated tests revealed that the lubrication lowers the wear rate of the pins and the discs but does not have a notable influence on COF. The solution strengthened ferritic ductile iron GJS-600-10 showed promising wear results against steel under continuous sliding motion. The disc wear rate of GJS-600-10 is equal to GJS-700-2 and a bit lower than that of GJS-600-3. This is adjoined with good results in the pin wear, where the wear rate of GJS-600-10 was comparable to GJS-600-3 and lower than that of GJS-700-2. Test results show that the influence of lubrication on wear resistance is more efficient with GJS-600-10 than with GJS-450-10. According to the test results of this thesis, the GJS-600-10 grade seems to perform well under this type of wear conditions. GJS-600-10 might be a future solution in applications where low wear and high friction are needed. GJS-600-10 is also a strong competitor to the GJS-700-2 grade, which was used as a reference material in HICON project. It is possible that some amount of fatigue wear is involved in the wear process. If this is the case, then the solution strengthened GJS-600-10 would be even more suitable material due to its high toughness properties.

REFERENCES

[1] Autere, Ingman, Tennilä, Valimotekniikka I, Insinööritieto OY, 1982.

[2] Rundman, K.B., Cast Irons, Encyclopedia of Materials, Science and Technology, pp 1003-1010, 2008.

[3] Ductile Iron Data, Rio Tinto & Titanium Inc., Canada, Quebec 1990.

[4] Morrogh, H., Williams, W.J., Journal of the Iron and Steel Institute, 158, 306, London, 1948.

[5] ISO/TR 10809-1:2009(E), Cast Irons – Part 1: Material and properties for design.

[6] EN ISO 945-1:2008, Microstructure of cast irons – Part 1: Graphite classification by visual analysis.

[7] prEN 1563:2009, Founding – Spheroidal graphite cast iron.

[8] Radzikowska, J.M., Metallography and Microstructures of Cast Iron, Metallography and Microstructures, Vol 9, ASM Handbook, ASM International, pp 565–587, 2004.

[9] Labreque, C., Gagné, M., Ductile Iron: Fifty years of continuous development, Canadian Metallugical Quarterly, Volume 37, No: 5, pp 343-378, published by Elsevier Science Ltd, 1998.

[10] ASM Handbook, Alloy Phase Diagrams, 3, 2-203, 1992.

[11] EN 1563:1997, Founding – Spheroidal graphite cast iron.

[12] Valuraudat ja valuteräkset, MET, Raaka-aine käsikirja, 2. painos, Tampere, 127-131, 2001.

[13] EN 1564+A1:2006, Founding – Austempered ductile cast irons.

[14] Bhushan Bharat. Introduction to Tribology. John Wiley & Sons. New York. 2002. 732 p.

[15] Braunovic, M., Myshkin, N., Konchits, V. Electrical contacts: Fundamentals, applications and technology. CRC Press 2007.

[16] Zum Gahr, K.H., Microstructure and Wear of Materials, Elsevier, 1987, Amsterdam.

[17] Bhushan Bharat. Modern Tribology Handbook. Vol. 1. CRC Press. New York. 2000. 765 p.

[18] Kivioja, S., Kivivuori, S. & Salonen, P. Tribologia – kitka, kuluminen ja voitelu. 3. edition. Helsinki, Otatieto. 2001. 351 s.

[19] Holm, R., Electric Contacts, 1946, Stockholm, Sweden.

[20] Archard, J.F., Contact and rubbing of flat surfaces, Journal of Applied Physics 25, 1953.

[21] Wood, R.J.K, University of Southampton, Tampere Wear Center: Wear Course Material, Oct. 2010.

[22] Rabinowicz, E., Friction and Wear of Materials, second edition, Wiley, New York, 1995.

[23] Suh, N., Saka, N., Fundamentals of Tribology, MIT Press, 1978.

[24] Braunovic, M., Myshkin, N., Konchits, V., Electrical contacts: Fundamentals, Applications and Technology, CRC Press, 2007.

[25] Peterson, M.B., Winer, W.O., Wear Control Handbook, ASME, 1980, New York.

[26] Lim, S.C., Ashby, M.F., Wear-mechanism Maps, Acta Metall. 35, 1-24, 1987.

[27] Lim, S.C., Ashby, M.F., Brunton, J.H., Wear-rate Transitions and Their Relationship to Wear Mechanisms, Acta Metall., 35, pp 1343-1348, 1987.

[28] Brown, J.R., Foseco Ferrous Foundryman's Handbook, 11th edition, Chapter 8 Special Purpose Cast Irons, 95-107, 2000.

[29] Islam, M.A., Haseeb, A.S.M.A., Kurny, A.S.W., Study of wear of as-cast and heat-treated spheroidal cast iron under dry sliding conditions, Wear 188, 61-65, 1995.

[30] Hirasata, K., Hayashi, K., Matsunami, H., Friction and wear of spheroidal graphite cast iron under severe sliding conditions, Tribology and Interface Engineering Series, Volume 41, pp 643-652, Elsevier, 2003.

[31] Lerner, Y.S., Wear Resistance of Ductile Irons, Journal of Materials Engineering and Performance, Volume 3, pp 403-408, 1994.

[32] Lerner, Y.S., Kingsbury, G.R., Wear Resistance Properties of Austempered Ductile Iron, Journal of Materials Engineering and Performance, Volume 7, pp 48-52, 1998.

[33] Abedi, H.R., Fareghi, A., Saghafian, Kheirandish, S.H, Sliding wear behavior of a ferritic-pearlitic ductile cast iron with different nodule count, Wear, 268, pp 622-628, 2010.

[34] Rebasa, N., Dommarco, R., Sikora, J., Wear resistance of high nodule count ductile iron, Wear, 253, pp 855-863, 2002.

[35] Dommarco, R., Sousa, M., Sikora, J., Abrasion resistance of high nodule count ductile iron with different matrix microstructures, Wear, 257, pp 1185-1192, 2004.

[36] Zimba, J., Transformation kinetics during the austempering of ductile iron and practical implications, Department of metallurgical engineering, University of Zimbabwe, 2000.

[37] Ahmadabadi, M., Ghasemi, H., Osia, M., Effects of successive austempering on the tribological behavior of ductile cast iron, Wear, 231, pp 293-300, 1999.

[38] EN 10264-1 2002, Steel wire and wire products – Steel wire for ropes – Part 1: General requirements.

[39] EN 10264-2 2002, Steel wire and wire products – Steel wire for ropes – Part 2: Cold drawn non alloy steel wire for ropes for general applications.

[40] ASTM G99-95a, Standard Test Method for Wear Testing with a Pin-On-Disk Apparatus.

APPENDIX 1: PROPERTIES OF THE SAMPLE DISCS

	Specimen no.	Material	Cast component	Bar no.	Casting date	Tensile Rm (N/mm^2)	Yield Rp $_{0,2}$ (N/mm^2)	Elongation (%)	Hardness (HB)	Nodular count ($_/mm^2$)
1	C10/1	GJS-1000-5	400002405	247	2010-10-19	1094	918	9,9	341	300
2	C10/2	GJS-1000-5	400002405	247	2010-10-19	1094	918	9,9	341	300
3	C10/3	GJS-1000-5	4021026	330	2010-11-18	1076	900	8,94	341	240
4	C10/4	GJS-1000-5	4021026	330	2010-11-18	1076	900	8,94	341	240
5	C10/5	GJS-1000-5	4021026	330	2010-11-18	1076	900	8,94	341	240
6	C10/6	GJS-1000-5	4021026	330	2010-11-18	1076	900	8,94	341	240
7	C10/7	GJS-1000-5	4021752	354	2010-11-30	1121	938	8,84	321	220
8	C10/8	GJS-1000-5	4021752	354	2010-11-30	1121	938	8,84	321	220
9	C12/1	GJS-1200-3	400002418	994/2	2010-10-05	1424	1237	4,08	429	200
10	C12/2	GJS-1200-3	400002418	994/2	2010-10-05	1424	1237	4,08	429	200
11	C12/3	GJS-1200-3	400002418	994	2010-10-05	1536	1362	4,32	444	180
12	C12/4	GJS-1200-3	400002418	994	2010-10-05	1536	1362	4,32	444	180
13	C12/5	GJS-1200-3	4020772	225	2010-10-12	1558	1405	4,46	461	240
14	C12/6	GJS-1200-3	4020772	225	2010-10-12	1558	1405	4,46	461	240
15	C4.5/1	GJS-450-10	4021027	232	2010-10-14	531	325	12,38	183	240
16	C4.5/2	GJS-450-10	4021027	232	2010-10-14	531	325	12,38	183	240
17	C4.5/3	GJS-450-10	4021028	233	2010-10-14	525	337	13,12	174	220
18	C4.5/4	GJS-450-10	4021028	233	2010-10-14	525	337	13,12	174	220
19	C4.5/5	GJS-450-10	4021027	291	2010-11-03	535	319	12,38	170	240
20	C4.5/6	GJS-450-10	4021027	291	2010-11-03	535	319	12,38	170	240
21	C4.5/7	GJS-450-10	4021027	299	2010-11-08	525	362	15,1	174	240
22	C4.5/8	GJS-450-10	4021027	299	2010-11-08	525	362	15,1	174	240
23	C4/1	GJS-400-15	4020984	260	2010-10-25	437	275	18,26	134	260
24	C4/2	GJS-400-15	4020984	260	2010-10-25	437	275	18,26	134	260
25	C4/3	GJS-400-15	4020977	314	2010-11-12	387	271	14,68	126	180
26	C4/4	GJS-400-15	4020977	314	2010-11-12	387	271	14,68	126	180
27	C4/5	GJS-400-15	4040984	331	2010-11-19	459	280	17,2	156	220
28	C4/6	GJS-400-15	4040984	331	2010-11-19	459	280	17,2	156	220
29	C5/1	GJS-500-7	4020864	234	2010-10-15	574	350	?	192	240
30	C5/2	GJS-500-7	4020864	234	2010-10-15	574	350	?	192	240
31	C5/3	GJS-500-7	4020940	248	2010-10-20	599	337	11,28	192	240
32	C5/4	GJS-500-7	4020940	248	2010-10-20	599	337	11,28	192	240
33	C5/5	GJS-500-7	4021534	249	2010-10-20	625	337	9,84	201	220
34	C5/6	GJS-500-7	4021534	249	2010-10-20	625	337	9,84	201	220
35	C5/7	GJS-500-7	4021678	303	2010-11-08	574	337	11,16	187	280
36	C5/8	GJS-500-7	4021678	303	2010-11-08	574	337	11,16	187	280
37	C5-14/1	GJS-500-14		1A	2010-11-30	555	488	17,9	184	233
38	C5-14/2	GJS-500-14		1B	2010-11-30	555	494	17,3	184	250
39	C5-14/3	GJS-500-14		1C	2010-11-30	554	490	18,8	183	225
40	C5-14/4	GJS-500-14		1D	2010-11-30	556	493	14,8	181	250
41	C6/1	GJS-600-3	4020824	236	2010-10-18	712	400	9,32	212	240
42	C6/2	GJS-600-3	4020824	236	2010-10-18	712	400	9,32	212	240
43	C6/3	GJS-600-3	4020821	297	2010-11-04	741	392	7,92	235	300
44	C6/4	GJS-600-3	4020821	297	2010-11-04	741	392	7,92	235	300
45	C6/5	GJS-600-3	4020824	298	2010-11-04	729	404	8,82	235	240
46	C6/6	GJS-600-3	4020824	298	2010-11-04	729	404	8,82	235	240
47	C6/7	GJS-600-3	4020887	308	2010-11-08	725	400	8,22	229	280
48	C6/8	GJS-600-3	4020887	308	2010-11-08	725	400	8,22	229	280
49	C6-10/1	GJS-600-10	33101269	96	2010-07-28	653	513	14,3	227	
50	C6-10/2	GJS-600-10	33101269	96	2010-07-28	653	513	14,3	227	
51	C6-10/3	GJS-600-10	33101269	95	2010-07-28	637	495	20,1	227	
52	C6-10/4	GJS-600-10	33101269	95	2010-07-28	637	495	20,1	227	
53	C6-10/5	GJS-600-10		3		602	539	10,88	207	
54	C6-10/6	GJS-600-10		3		602	539	10,88	207	
55	C6-10/7	GJS-600-10		4		600	523	10,86	212	
56	C6-10/8	GJS-600-10		4		600	523	10,86	212	
57	C7/1	GJS-700-2	4020892	235	2010-10-15	759	490	4,52	269	220
58	C7/2	GJS-700-2	4020892	235	2010-10-15	759	490	4,52	269	220
59	C7/3	GJS-700-2	4020978	243	2010-10-19	809	539	4,8	262	400
60	C7/4	GJS-700-2	4020978	243	2010-10-19	809	539	4,8	262	400
61	C7/5	GJS-700-2	4020978	304	2010-11-08	775	525	3,16	277	220
62	C7/6	GJS-700-2	4020978	304	2010-11-08	775	525	3,16	277	220
63	C7/7	GJS-700-2	4021123	305	2010-11-08	800	525	4,48	269	
64	C7/8	GJS-700-2	4021123	305	2010-11-08	800	525	4,48	269	
65	C9/1	GJS-900-7	4020829	241	2010-10-19	968	750	10,54	302	320
66	C9/2	GJS-900-7	4020829	241	2010-10-19	968	750	10,54	302	320
67	C9/3	GJS-900-7	4020829	242	2010-10-19	1017	747	11,94	302	260
68	C9/4	GJS-900-7	4020829	242	2010-10-19	1017	747	11,94	302	260
69	C9/5	GJS-900-7	4020828	257	2010-10-22	962	750	10,48	293	220
70	C9/6	GJS-900-7	4020828	257	2010-10-22	962	750	10,48	293	220

APPENDIX 2A: DRAWING OF THE PIN HOLDER

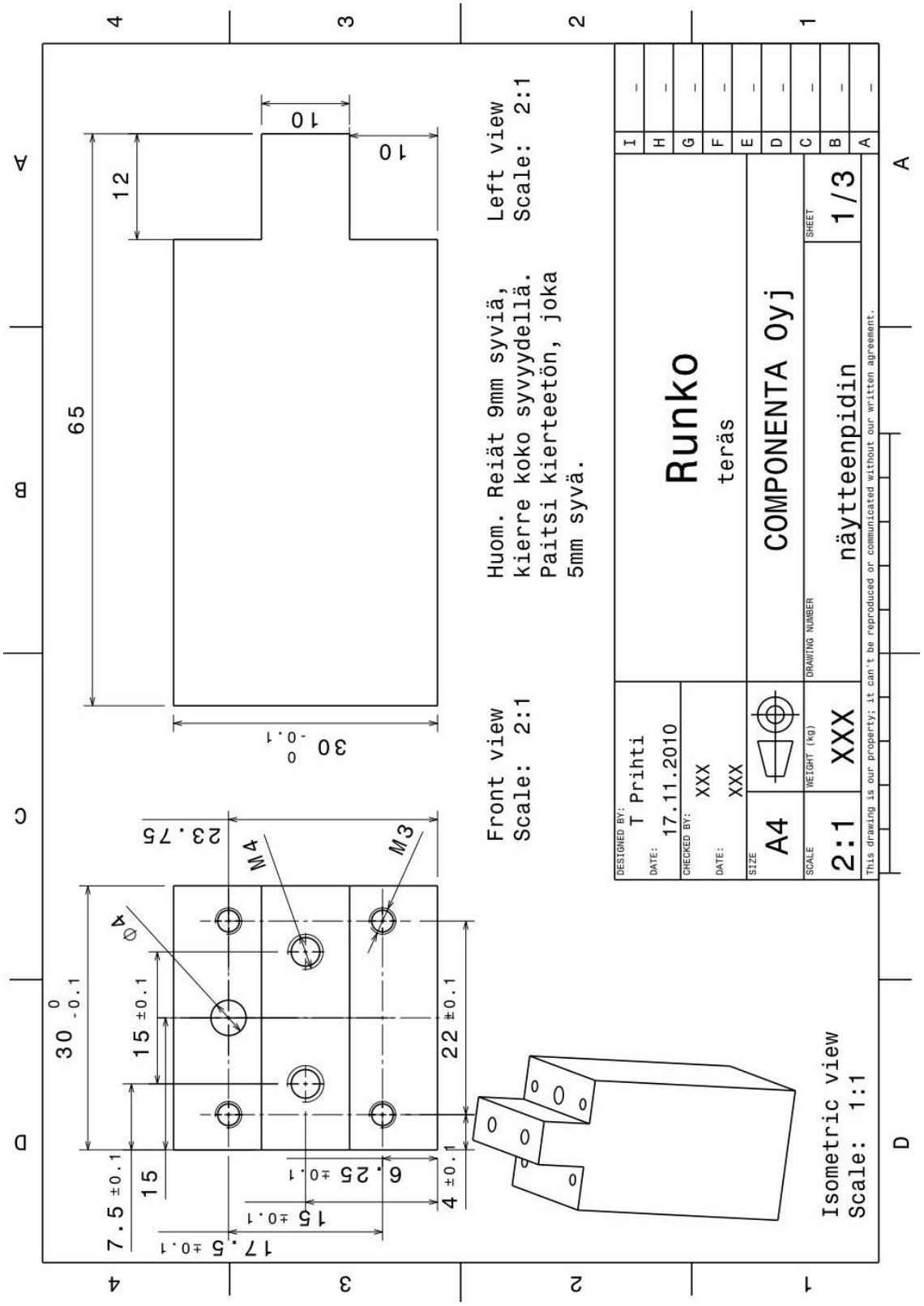

APPENDIX 2B: DRAWING OF THE PIN HOLDER

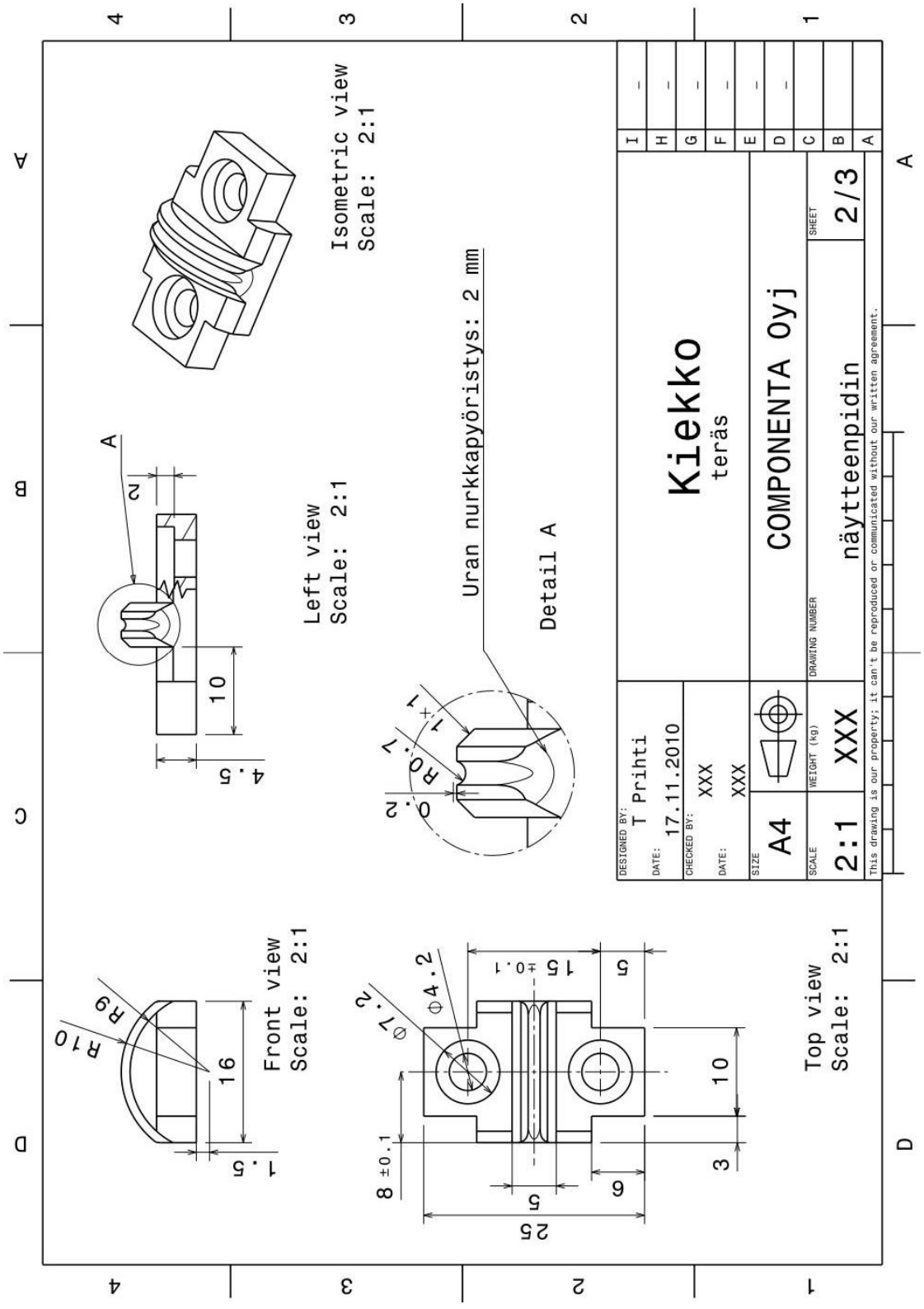

APPENDIX 2C: DRAWING OF THE PIN HOLDER

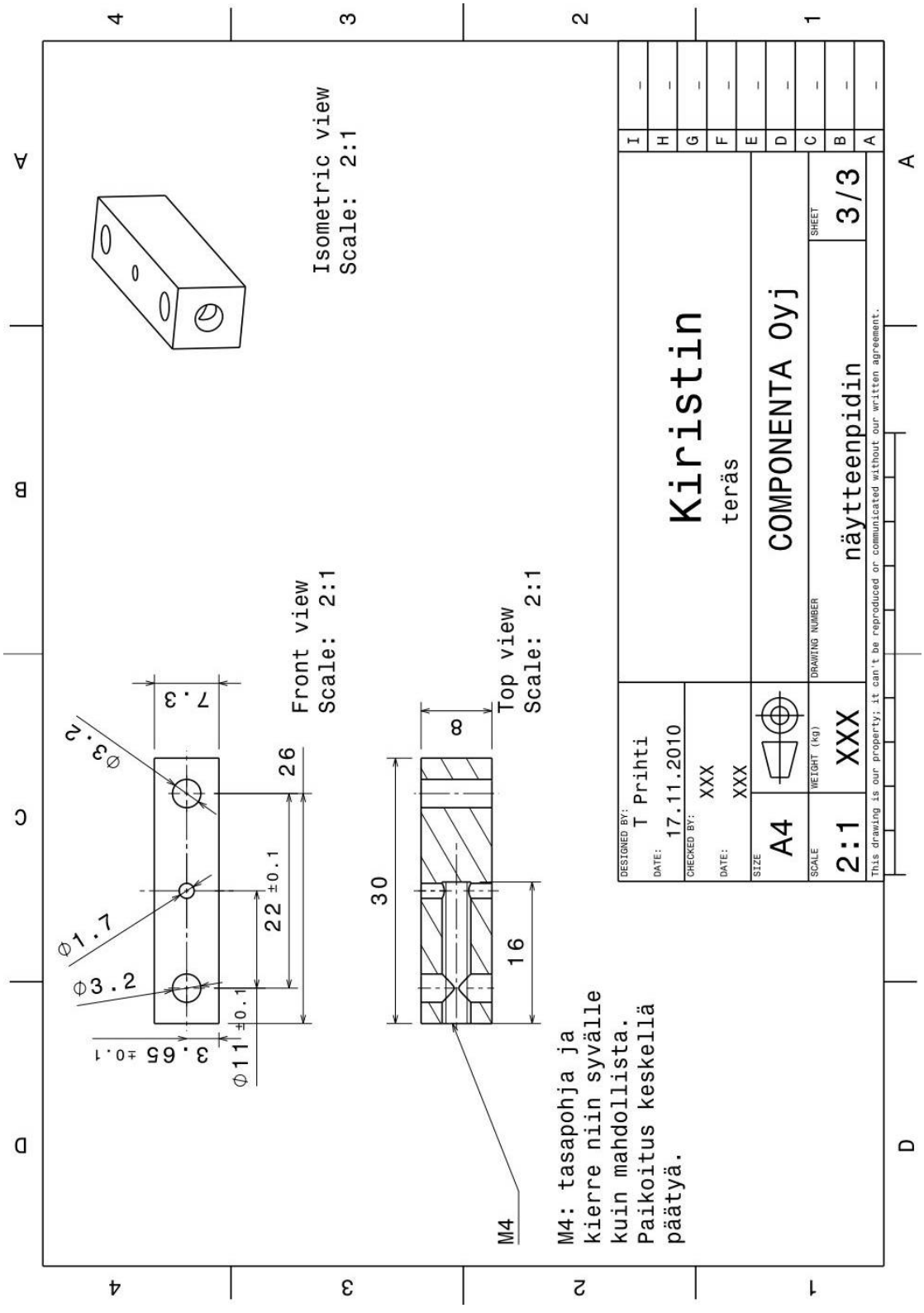

APPENDIX 3A: DRY SLIDING TEST RESULTS

Test code	Date	Disc sample	Material	x (mm)	y (mm)	h (mm)	Pin wear (mm^3)	COF	Disc wear (mm^3)	Tensile Rm (N/mm^2)	Yield $Rp_{0,2}$ (N/mm^2)	Elongation (%)	Hardness (HB)	Nodular count ($/mm^2$)
Koe 2	14.12.2010	C4/2	GJS-400-15	0,551	0,145	0,015	0,002518	0,197	-0,00030	437	275	18,26	134	260
Koe 32	26.1.2011	C4/3	GJS-400-15	0,447	0,129	0,012	0,001459	0,221	0,00380	387	271	14,68	126	180
Koe 27	25.1.2011	C4/4	GJS-400-15	0,484	0,129	0,012	0,001580	0,241	0,00404	387	271	14,68	126	180
Average			GJS-400-15				0,001852	0,220	0,00251	404	272	15,87	129	207
Koe 4	16.12.2010	C4.5/2	GJS-450-10	0,427	0,116	0,010	0,001012	0,203	0,00960	531	325	12,38	183	240
Koe 19	12.1.2011	C4.5/3	GJS-450-10	0,511	0,137	0,014	0,001982	0,217	0,00002	525	337	13,12	174	220
Koe 16	11.1.2011	C4.5/7	GJS-450-10	0,554	0,141	0,014	0,002364	0,226	0,00201	525	362	15,10	174	240
Average			GJS-450-10				0,001786	0,215	0,00388	527	341	13,53	177	233
Koe 7	17.12.2010	C5/1	GJS-500-7	0,435	0,103	0,008	0,000720	0,150	0,00279	574	350		192	240
Koe 5	16.12.2010	C5/2	GJS-500-7	0,617	0,160	0,018	0,003818	0,256	0,00503	574	350		192	240
Koe 8	17.12.2010	C5/8	GJS-500-7	0,573	0,155	0,017	0,003259	0,232	0,00721	574	337	11,16	187	280
Average			GJS-500-7				0,003538	0,244	0,00612	574	346	11,16	190	253
Koe 29	25.1.2011	C5-14/1	GJS-500-14	0,475	0,126	0,011	0,001436	0,214	-0,00015	555	488	17,88	184	233
Koe 33	26.1.2011	C5-14/2	GJS-500-14	0,579	0,165	0,020	0,003965	0,269	0,00094	555	494	17,28	184	250
Koe 35	26.1.2011	C5-14/3	GJS-500-14	0,616	0,167	0,020	0,004388	0,274	0,00064	554	490	18,76	183	225
Average			GJS-500-14				0,004176	0,272	0,00079	555	491	17,97	184	236
Koe 15	11.1.2011	C6/3	GJS-600-3	0,618	0,172	0,021	0,004759	0,292	0,01078	741	392	7,92	235	300
Koe 21	12.1.2011	C6/4	GJS-600-3	0,558	0,154	0,017	0,003106	0,269	0,00662	741	392	7,92	235	300
Koe 9	17.12.2010	C6/5	GJS-600-3	0,601	0,160	0,018	0,003717	0,277	0,00410	729	404	8,82	235	240
Average			GJS-600-3				0,003861	0,279	0,00717	737	396	8,22	235	280

APPENDIX 3B: DRY SLIDING TEST RESULTS

Test code	Date	Disc sample	Material	x (mm)	y (mm)	h (mm)	Pin wear (mm^3)	COF	Disc wear (mm^3)	Tensile Rm (N/mm^2)	Yield $Rp_{0,2}$ (N/mm^2)	Elongation (%)	Hardness (HB)	Nodular count ($/mm^2$)
Koe 34	26.1.2011	C6-10/1	GJS-600-10	0,655	0,175	0,022	0,005340	0,311	0,01069	653	513	14,30	227	
Koe 30	25.1.2011	C6-10/2	GJS-600-10	0,549	0,149	0,016	0,002743	0,301	0,00230	653	513	14,30	227	
Koe 38	27.1.2011	C6-10/7	GJS-600-10	0,608	0,157	0,018	0,003530	0,313	0,00375	600	523	10,86		
Average			GJS-600-10				0,003871	0,308	0,00558	635	516	13,15	227	
Koe 12	11.1.2011	C7/1	GJS-700-2	0,657	0,174	0,022	0,005249	0,269	0,00554	759	490	4,52	269	220
Koe 13	11.1.2011	C7/2	GJS-700-2	0,647	0,171	0,021	0,004882	0,266	0,00422	759	490	4,52	269	220
Koe 14	11.1.2011	C7/3	GJS-700-2	0,763	0,200	0,029	0,009326	0,322	0,00674	809	539	4,80	262	400
Average			GJS-700-2				0,006486	0,286	0,00550	776	506	4,61	267	280
Koe 17	11.1.2011	C9/1	GJS-900-7	0,855	0,222	0,036	0,014321	0,404	0,00396	968	750	10,54	302	320
Koe 20	12.1.2011	C9/2	GJS-900-7	0,914	0,238	0,042	0,019013	0,431	-0,00314	968	750	10,54	302	320
Koe 22	12.1.2011	C9/5	GJS-900-7	0,858	0,216	0,034	0,013310	0,375	-0,00619	962	750	10,48	293	220
Average			GJS-900-7				0,015548	0,403	-0,00179	966	750	10,52	299	287
Koe 24	13.1.2011	C10/2	GJS-1000-5	0,826	0,223	0,036	0,014038	0,372	-0,00556	1094	918	9,90	341	300
Koe 28	25.1.2011	C10/6	GJS-1000-5	0,857	0,221	0,036	0,014126	0,440	0,00540	1076	900	8,94	341	240
Koe 36	26.1.2011	C10/7	GJS-1000-5	0,895	0,236	0,041	0,018090	0,442	-0,00126	1121	938	8,84	321	220
Average			GJS-1000-5				0,015418	0,418	-0,00047	1097	919	9,23	334	253
Koe 3	15.12.2010	C12/1	GJS-1200-3	0,880	0,227	0,038	0,015872	0,386	-0,00117	1424	1237	4,08	429	200
Koe 1	14.12.2010	C12/2	GJS-1200-3	0,936	0,239	0,042	0,019739	0,422	-0,00204	1424	1237	4,08	429	200
Koe 10	10.1.2011	C12/4	GJS-1200-3	0,870	0,225	0,037	0,015222	0,379	-0,00821	1536	1362	4,32	444	180
Average			GJS-1200-3				0,016944	0,396	-0,00381	1461	1279	4,16	434	193

APPENDIX 4: LUBRICATED SLIDING TEST RESULTS

Test code	Date	Disc sample	Material	x (mm)	y (mm)	h (mm)	Pin wear (mm^3)	COF	Disc wear (mm^3)	Tensile Rm (N/mm^2)	Yield Rp 0,2 (N/mm^2)	Elongation (%)	Hardness (HB)	Nodular count ($/mm^2$)
Koe 6	16.12.2010	C4.5/1	GJS-450-10	0,785	0,205	0,031	0,010408	0,255	0,02591	531	325	12,38	183	240
Koe 23	12.1.2011	C4.5/4	GJS-450-10	0,643	0,174	0,022	0,0051444	0,302	0,02050	525	337	13,12	174	220
Average			GJS-450-10				0,007776	0,278	0,02321	528	331	12,75	179	230
Koe 37	26.1.2011	C6-10/3	GJS-600-10	0,647	0,173	0,022	0,005073	0,298	0,00618	637	495	20,1	227	
Koe 39	27.1.2011	C6-10/4	GJS-600-10	0,715	0,185	0,025	0,006895	0,314	0,01208	637	495	20,1	227	
Average			GJS-600-10				0,005984	0,306	0,00913	637	495	20,10	227	
Koe 18	11.1.2011	C7/7	GJS-700-2	0,452	0,122	0,011	0,001230	0,134	0,00116	800	525	4,48	269	
Koe 26	13.1.2011	C7/8	GJS-700-2	1,207	0,302	0,069	0,052366	0,279	0,02156	800	525	4,48	269	
Average			GJS-700-2				0,026798	0,207	0,01136	800	525	4,48	269	
Koe 11	10.1.2011	C10/1	GJS-1000-5	0,722	0,185	0,025	0,006935	0,244	0,00731	1094	918	9,9	341	300
Koe 31	25.1.2011	C10/4	GJS-1000-5	1,478	0,372	0,107	0,122993	0,439	0,07374	1076	900	8,94	341	240
Average			GJS-1000-5				0,064964	0,342	0,04052	1085	909	9,42	341	270